Proton decay matrix elements with domain-wall fermions

Y. Aoki,[1,*] C. Dawson,[2] J. Noaki,[3,†] and A. Soni[4]

[1]*Physics Department, University of Wuppertal, Gaussstrasse 20, 42119 Wuppertal, Germany*
[2]*RIKEN-BNL Research Center, Brookhaven National Laboratory, Upton, New York 11973, USA*
[3]*School of Physics and Astronomy, University of Southampton, Southampton, SO17 1BJ, United Kingdom*
[4]*Physics Department, Brookhaven National Laboratory, Upton, New York 11973, USA*

(Received 20 September 2006; published 25 January 2007)

Hadronic matrix elements of operators relevant to nucleon decay in grand unified theories are calculated numerically using lattice QCD. In this context, the domain-wall fermion formulation, combined with nonperturbative renormalization, is used for the first time. These techniques bring reduction of a large fraction of the systematic error from the finite lattice spacing. Our main effort is devoted to a calculation performed in the quenched approximation, where the direct calculation of the nucleon to pseudoscalar matrix elements as well as the indirect estimate of them from the nucleon to vacuum matrix elements are performed. First results, using two flavors of dynamical domain-wall quarks for the nucleon to vacuum matrix elements, are also presented to address the systematic error of quenching, which appears to be small compared to the other errors. Our results suggest that the representative values for the low-energy constants from the nucleon to vacuum matrix elements are given as $|\alpha| \simeq |\beta| \simeq 0.01$ GeV^3. For a more reliable estimate of the physical low-energy matrix elements, it is better to use the relevant form factors calculated in the direct method. The direct method tends to give a smaller value of the form factors, compared to the indirect one, thus enhancing the proton lifetime; indeed, for the π^0 final state the difference between the two methods is quite appreciable.

DOI: 10.1103/PhysRevD.75.014507 PACS numbers: 12.38.Gc, 11.30.Rd, 12.10.Dm

I. INTRODUCTION

In the standard model, baryon number is conserved up to a very good approximation. While it is broken (only) by the electroweak anomaly, the size of breaking is extremely small so that baryon number violation would be extremely difficult to observe in any high-energy experiment. The conservation of baryon number happens to be exact in the classical level in the standard model. However, it is not a consequence of the underlying fundamental symmetries, e.g. gauge and Lorentz symmetries. In general, baryon number is not protected once we extend the gauge groups of the standard model to larger symmetry groups. The existence of the baryon number violating interaction makes protons unstable. This particular phenomenon, proton decay, or in general, nucleon decay, is one of the most decisive signals that proves the nature has larger fundamental symmetry than that of the standard model. Grand unified theories (GUTs) [1,2], with or without supersymmetry, possess such a feature.

Although proton decay has been searched for in the deep mine experiments for more than a decade, it has not been observed [3]. The lower bound of the proton lifetime from the experiments has provided an important stringent constraint on the GUT models. In fact, the simplest minimal supersymmetric (SUSY) GUT with $SU(5)$ gauge group is almost surely excluded [4,5].

At low energies, the processes that allow nucleon decay may be represented in terms of a low-energy effective Hamiltonian made up of standard model fields. This effective Hamiltonian will be dominated by the operators of lowest dimension. The requirement that the low-energy effective theory has the same symmetry as the standard model is strong enough to constrain the form of the possible operators in the effective Hamiltonian [8–10]. The operators consist of three quarks and one lepton field as $(\bar{q}^c q)(\bar{l}^c q)$, which lead to a decay of a nucleon to a pseudoscalar and an antilepton. As the low-energy hadrons are involved in the decay, this is a highly nonperturbative process, and so lattice QCD provides an ideal tool to analyze it.

Since it is difficult to calculate the hadronic matrix element $\langle PS|(\bar{q}^c q)q|N\rangle$ of the three-quark operator with initial nucleon (N) and final pseudoscalar (PS) states, various QCD model approaches were used to calculate the nucleon to vacuum matrix element $\langle 0|(\bar{q}^c q)q|N\rangle$, which in turn gives $\langle PS|(\bar{q}^c q)q|N\rangle$ with the help of chiral perturbation theory. In the 1980's many calculations of the matrix elements [11–18] were reported. These calculations varied by a factor of $O(10)$ between the smallest and largest estimates (see [18] and Table VI). As the partial width of the decay is proportional to the matrix elements squared, different model calculations lead to a factor of $O(100)$ difference in proton lifetime.

The first calculations [19–21] using lattice QCD were performed in the late 1980's. These calculations also took the approach of calculating the nucleon to vacuum matrix elements, using chiral perturbation theory to infer the final result. The nucleon to vacuum matrix elements obtained in

*Present address: RIKEN-BNL Research Center, Brookhaven National Laboratory, Upton, NY 11973.
†Institute of Particle and Nuclear Studies, KEK, Ibaraki 305-0801, Japan.

these studies disagreed as well, with a factor of about 5 difference between the smallest [21] and largest [19] estimates.

There are various sources of systematic errors involved in such calculations, one of which is the large range extrapolation of the matrix elements in the quark mass. As the matrix elements are used as the low-energy constants of the chiral Lagrangian, they must be obtained in the chiral limit. These original lattice studies necessarily used unphysically heavy values of the up and down quark masses. In fact, the values used were typically of the order of the mass of the physical strange quark.

Another source of error comes from measuring the lattice scale. Since the low-energy constants measured have mass dimension three, their error—when quoted in physical units—receives a contribution equal to 3 times the error on this scale. There are various ways of extracting the lattice scale which need not agree at finite lattice spacing, or when working in the quenched approximation. Moreover, some conventional ways to set the lattice scale, such as using the ρ meson or the nucleon mass as an input again, require a large extrapolation in the mass to reach the physical point. It is important to note that all the calculations performed up to now used unimproved Wilson fermions, a formulation known to have large scaling violations. It is not surprising that a moderate difference in the lattice cutoff leads to a large difference in the low-energy constants.

Operator renormalization is another source of systematic error. The operators which mediate the nucleon decay must be renormalized in some renormalization scheme. This must be the same renormalization scheme that was used for the calculation of the Wilson coefficients for the effective Hamiltonian, and is usually the $\overline{\mathrm{MS}}$ scheme. The common way to perform this calculation has been to use lattice perturbation theory, which has a poor convergence property, leading to a large systematic error.

There is one important systematic error, which neither the model nor the lattice calculations in the 1980's address: even if one gets the correct value of the low-energy constants, the matrix element for the decay could have an appreciable error. The reason is that the pion resulting from the decay has, in the center of mass (CM) frame, a momentum around half of the nucleon mass, where the leading order chiral expansion may not be a good approximation.

The (more recent) JLQCD work [22] was better at addressing many of these systematics compared to the old results: they employed smaller quark masses, and used an improved lattice perturbation theory. Most importantly, the first reliable direct measurement for the nucleon to pseudoscalar matrix elements was performed. However, the calculation was still performed in the quenched approximation, and made use of the unimproved Wilson action. Later, a joint collaboration including some of the original JLQCD members addressed the issue of the scaling violations in the restricted case of the nucleon to vacuum matrix elements [23]. It appeared that the value JLQCD got at a finite lattice spacing was larger by almost a factor 2 than that in the continuum limit, showing the particular difficulty in taking the continuum limit with the unimproved Wilson fermions.

In this paper we calculate the nucleon-decay matrix elements in an approach similar to JLQCD, but with three key differences: we use domain-wall fermions, which preserve chiral symmetry to a very high accuracy (and so are expected to have much reduced scaling violations); we use a nonperturbative renormalization scheme; and we also investigate the effects of moving away from the quenched approximation. As mentioned previously, all the works which have been done so far for nucleon decay used the quenched approximation wherein the quark loops in the propagation of the gluons are neglected. Although it has been shown that the light flavored hadron spectrum is reproduced by the quenched approximation within a 10% difference of experiment [24], the systematic error due to this approximation is process dependent and, in general, uncontrollable. We present the first study of the quenching error by calculating the nucleon to vacuum matrix elements using unquenched u, d quarks and comparing to the quenched result. As a result of these differences, an appreciable reduction of the systematic error is expected.

This paper is organized as follows: in Sec. II we summarize the general properties of the baryon number violating operator and the nucleon-decay matrix elements. Section III discusses the operator property in view of the renormalization and gives the detail of how to apply the nonperturbative renormalization scheme to the nucleon-decay operator. The calculation of nucleon-decay matrix elements with the quenched approximation is shown in Sec. IV. The estimate of the nucleon to vacuum matrix elements with unquenching u, d quarks is given in Sec. V. Section VI is devoted to the conclusions. Some results obtained in earlier stages of this work have been reported in Refs. [25–27].

We use the Euclidean lattice formulation, so the metric and gamma matrices should be taken as Euclidean. Dimensional quantities are often written in the lattice units (a). We avoid writing "a" explicitly in most cases.

II. GENERAL DESCRIPTION

In this section we describe the operators and matrix elements to calculate, and their theoretical background. We give an overview of the lattice calculation setup, which in the later sections will be discussed in detail.

A. Properties of operators and matrix elements

The general type of nucleon-decay operator that appears in the low-energy effective Hamiltonian is constrained by

the symmetries of the standard model, $SU(3)_c \times SU(2)_L \times U(1)_Y$ [8,9]. The quark part must contain three quark fields, as the $SU(3)_c$ singlet made of $3 \times 3 \times 3$ is the lowest dimensional baryon number violating operator which is invariant under $SU(3)_c$. Another fermion field (lepton or antilepton) is necessary to make the operator Lorentz invariant. The $SU(2)_L \times U(1)_Y$ symmetry rules out the possibility of having the antilepton field in the operator, and restricts the flavor/chirality combination to four types [10]. In the notation of Weinberg [8], Abbott and Wise [10], these operators read [28]

$$O^{(1)}_{abcd} = (D^i_a, U^j_b)_R (q^{k\alpha}_c, l^\beta_d)_L \epsilon^{ijk} \epsilon^{\alpha\beta}, \tag{1}$$

$$O^{(2)}_{abcd} = (q^{i\alpha}_a, q^{j\beta}_b)_L (U^k_c, l_d)_R \epsilon^{ijk} \epsilon^{\alpha\beta}, \tag{2}$$

$$\tilde{O}^{(4)}_{abcd} = (q^{i\alpha}_a, q^{j\beta}_b)_L (q^{k\gamma}_c, l^\delta_d)_L \epsilon^{ijk} \epsilon^{\alpha\beta} \epsilon^{\gamma\delta}, \tag{3}$$

$$O^{(5)}_{abcd} = (D^i_a, U^j_b)_R (U^k_c, l_d)_R \epsilon^{ijk}, \tag{4}$$

where l is the generic lepton field, q is the left handed quark field, and U and D denote up and down type right handed quarks. a, b, c, d are generation numbers; i, j, k are $SU(3)$ color labels; and $\alpha, \beta, \gamma, \delta$ are $SU(2)$ indices. The inner product $(x, y)_{R/L}$ is defined as $(x, y)_{R/L} = x^T C P_{R/L} y$, where C is the charge conjugation matrix and $P_{R/L}$ is the right/left handed projection matrix. The vector and tensor Dirac matrices have been eliminated in the expression by Fierz rearrangement. These dimension-six operators [29] are the lowest dimensional operators that appear in the low-energy effective Hamiltonian written in terms of standard model particles. Higher dimensional operators are suppressed by inverse powers of the heavy mass scale characteristic of the fundamental high-energy theory (e.g. M_X for GUTs). As is evident from the form of the operator, it breaks baryon number (B), but preserves baryon minus lepton number ($B - L$), leading to a decay of the nucleon to a pseudoscalar and an antilepton.

The general form of the three-quark part of the operator, which transforms as a spinor, is

$$\mathcal{O}^{\Gamma\Gamma'}_{uds} = (ud)_\Gamma s_{\Gamma'} = \epsilon^{ijk} (u^{iT} C P_\Gamma d^j) P_{\Gamma'} s^k, \tag{5}$$

where $\Gamma(\Gamma')$ can be either R or L. u, d, and s are quark fields not necessarily labeling the real u, d, s flavors. From the form of the operator, it is evident that the proton or neutron cannot decay to a final state that has strangeness $S < 0$. Thus, processes such as $p \to \bar{K}^0 + l^+$ are disallowed. The trivial constraint that the mass of the pseudoscalar (PS) is below that of the nucleon (N), $m_{PS} < m_N$, requires the final state to be one of π^0, $\pi^\pm$, K^0, K^+, or η. Hence the real physical flavor of a quark in Eq. (5) is one of the three lightest, u, d, s.

We calculate the hadronic matrix element with the nucleon and the allowed pseudoscalar states,

$$\langle PS; \vec{p} | \mathcal{O}^{\Gamma\Gamma'} | N; \vec{k}, s \rangle, \tag{6}$$

where $\vec{p}$ and $\vec{k}$ are spatial momenta of the pseudoscalar and nucleon, respectively, and $s = \pm 1/2$ is the spin of the nucleon. Parity transformation yields a relation between different chirality matrix elements:

$$\langle PS; \vec{p} | \mathcal{O}^{R/LL} | N; \vec{k}, s \rangle = \gamma_4 \langle PS; -\vec{p} | \mathcal{O}^{L/RR} | N; -\vec{k}, s \rangle. \tag{7}$$

For the range of accuracy that is expected from our calculation, it is sufficient to assume isospin symmetry, which further reduces the number of independent matrix elements. Following Ref. [22], here we list 14 matrix elements and their "isospin partners" obtained by exchanging u and d:

$$\langle \pi^0 | (ud)_{R/L} u_L | p \rangle = \langle \pi^0 | (du)_{R/L} d_L | n \rangle, \tag{8}$$

$$\langle \pi^+ | (ud)_{R/L} d_L | p \rangle = -\langle \pi^- | (du)_{R/L} u_L | n \rangle, \tag{9}$$

$$\langle K^0 | (us)_{R/L} u_L | p \rangle = -\langle K^+ | (ds)_{R/L} d_L | n \rangle, \tag{10}$$

$$\langle K^+ | (us)_{R/L} d_L | p \rangle = -\langle K^0 | (ds)_{R/L} u_L | n \rangle, \tag{11}$$

$$\langle K^+ | (ud)_{R/L} s_L | p \rangle = -\langle K^0 | (du)_{R/L} s_L | n \rangle, \tag{12}$$

$$\langle K^+ | (ds)_{R/L} u_L | p \rangle = -\langle K^0 | (us)_{R/L} d_L | n \rangle, \tag{13}$$

$$\langle \eta | (ud)_{R/L} u_L | p \rangle = -\langle \eta | (du)_{R/L} d_L | n \rangle. \tag{14}$$

Our interpolating field for each hadron state is summarized in Appendix A. The negative signs on the right-hand sides (rhs) of Eqs. (8)–(14) appear from the transformation of the interpolating fields $J_{\pi^0} \to -J_{\pi^0}$ and $\bar{J}_p \to -\bar{J}_n$ by interchanging u and d. There is a relation between final π^0 and final $\pi^\pm$ matrix elements in the isospin limit,

$$\langle \pi^+ | (ud)_{R/L} d_L | p \rangle = \sqrt{2} \langle \pi^0 | (ud)_{R/L} u_L | p \rangle. \tag{15}$$

We call the left-hand sides (lhs) of Eqs. (8) and (10)–(14) the principal matrix elements. In the quenched simulation, we are going to calculate these 12 principal matrix elements. All the other matrix elements are obtained from the principal matrix elements using Eqs. (7)–(15). Note, however, that the flavor $SU(3)$ breaking effect of η is not treated in this paper [30]. A nucleon to pseudoscalar decay is characterized by its initial three momentum $\vec{k}$, spin $s = \pm 1/2$, and final momentum $\vec{p}$. By Lorentz covariance, the matrix element is required to have the form [22]

$$\langle PS; \vec{p} | \mathcal{O}^{R/LL} | N; \vec{k}, s \rangle = P_L [W_0^{R/LL}(q^2) - i \not{q} W_q^{R/LL}(q^2)] u_N(\vec{k}, s), \tag{16}$$

where u_N is the nucleon spinor. The form factors W_0 and W_q are functions of the square of the momentum transfer

$q_\mu = k_\mu - p_\mu$. For the physical decay, this is the momentum of the lepton. However, on the lattice we work with unphysical values of the masses and momentum transfer, and then extrapolate to the physical point. In this case, W_0 and W_q are the functions of m_N, m_{PS}, and q^2. For the range of masses and momenta used in our simulation, the two terms in the square brackets seem to be of the same order. This fact implies that the second term is negligible in the physical amplitude due to the on-shell condition on the lepton ($-q^2 = m_l^2$) [31]. Hence, W_0 is called relevant and W_q is an irrelevant form factor. As $-q^2 = m_l^2 \simeq 0$, $W_0(0)$ is the final target of our calculation. The parity condition, Eq. (7), implies the relation between form factors with different chirality as

$$W_x^{R/LR}(q^2) = W_x^{L/RL}(q^2), \tag{17}$$

for $x = 0, q$. Note that parity holds only after the statistical average over lattice gauge field configurations. On a single gauge configuration, the rhs and lhs of Eq. (17) generally differ, and we can take their average to get better statistics, which is done in our analysis.

Once the form factor is calculated, the partial width of the $p \to PS + \bar{l}$ decay is obtained as

$$\Gamma(p \to PS + \bar{l}) = \frac{m_p}{32\pi^2}\left[1 - \left(\frac{m_{PS}}{m_p}\right)^2\right]^2 \times \left|\sum_i C^i W_0^i(p \to PS)\right|^2, \tag{18}$$

where m_p (m_{PS}) denotes the proton (pseudoscalar) mass, and we have set the lepton mass to zero. C^i are the Wilson coefficients of the dimension-six operator in the low-energy effective Hamiltonian,

$$\mathcal{L}_6 = \sum_i C^i[(qq)(ql)]^i = -\sum_i C^i[\bar{l}^c \mathcal{O}_{qqq}]^i. \tag{19}$$

The index i distinguishes the type (flavor and chirality) of the three-quark operator $\mathcal{O}_{qqq}$, which is one of those in the matrix elements, Eqs. (8)–(14), as well as the type of lepton. While C_i and W_0^i depend on the renormalization scheme and scale, the dependence cancels out in the product. In this work we use a renormalization scale $\mu = 2$ GeV and the $\overline{\text{MS}}$ scheme with the naive dimensional regularization (NDR) for W_0^i. With W_0^i calculated in this work, and a knowledge of C_i, which depend on the particular GUT model, the proton lifetime can be estimated through Eq. (18).

B. Usage of chiral perturbation theory

In this work we discuss the calculation of the form factors for the principal matrix elements by means of numerical lattice simulations. To obtain the results at the physical kinematics in terms of quark masses and pseudoscalar momentum, it is necessary to know the dependence of the form factors on these parameters, especially for the u, d quark masses as these are not attainable on the lattice with the present algorithmic and computational resources. Chiral perturbation theory (χPT) gives such information. The tree-level result for the form factors of the nucleon decay are available [22]. The "direct method," which uses three-point functions and various two-point functions, estimates the matrix elements for the kinematics of the particular lattice simulation. Then they are extrapolated/interpolated to the physical kinematics with the help of χPT.

The chiral Lagrangian of the nucleon decay [32] involves only two additional low-energy parameters to the ordinary three-flavor baryon chiral Lagrangian at leading order. Measuring these parameters on the lattice and combining with the other parameters of the baryon chiral Lagrangian, all the matrix elements of nucleon decay can, in principle, be calculated. For the proton to π^0 decay as an example, the relevant form factors read

$$W_0^{RL}(p \to \pi^0) = \alpha(1 + D + F)/\sqrt{2}f, \tag{20}$$

$$W_0^{LL}(p \to \pi^0) = \beta(1 + D + F)/\sqrt{2}f, \tag{21}$$

where f is the tree-level pion decay constant with a normalization such that the experimental value is $f_\pi \simeq 131$ MeV. D and F are the couplings of baryons to the axial current, where the sum of them gives the nucleon axial charge: $D + F = g_A$. α and β are specific to the nucleon decay which can be calculated at leading order through the proton to vacuum matrix element of the operators,

$$\alpha P_L u_p = \langle 0|\mathcal{O}_{udu}^{RL}|p\rangle, \qquad \beta P_L u_p = \langle 0|\mathcal{O}_{udu}^{LL}|p\rangle, \tag{22}$$

$$\alpha P_R u_p = -\langle 0|\mathcal{O}_{udu}^{LR}|p\rangle, \qquad \beta P_R u_p = -\langle 0|\mathcal{O}_{udu}^{RR}|p\rangle, \tag{23}$$

where Eq. (23) is obtained from Eq. (22) by parity transformation. We fix the phase definition such that α and β are real and $\alpha < 0$. As we will later describe, we observe $\alpha + \beta \simeq 0$, which is expected because of the relation

$$(\alpha + \beta)u_p = -\langle 0|\epsilon^{ijk}(u^{Ti} C d^j)\gamma_5 u^k|p\rangle, \tag{24}$$

which vanishes in the nonrelativistic limit and is known to be quite small even at small quark masses [33].

Reduction formulas similar to Eqs. (20) and (21) are available for all the principal matrix elements [22,32]. These are summarized in Appendix B. This way of calculating the matrix elements is referred to as the "indirect method." It has to be noted that the indirect method can have a sizable systematic error, which is difficult to estimate reliably:

(1) In the $SU(3)_f$ baryon chiral Lagrangian, there are four parameters which control the flavor $SU(3)$ breaking effects. Two parameters are used to match the baryon masses, and enter the nucleon-decay

matrix elements through baryon masses. The other two contribute for the nucleon to pseudoscalar matrix element we wish to extract (and calculate in the direct method), but do not contribute to the nucleon to vacuum matrix elements required in the indirect method. As we have no means to estimate their values, we set these parameters, named b_i ($i = 1, 2$) in Refs. [22,32], as $b_i = 0$ as is standard for such calculations. However, they can naturally be $O(1)$. Setting $|b_i| = 1$ for a test, the contribution of the breaking term to the relevant form factors is estimated as 5%–30% for $N \to K$ decays. The worst case is $\langle \eta | (ud)_R u_L | p \rangle$, where the contribution is as large as 200% [32,34]. For $N \to \pi$ the effect of these parameters should be negligible.

(2) Even if flavor violation effects were small, i.e., effects of b_i were negligible, there could be an appreciable systematic error from the usage of the lowest order χPT. This is due to the large energy of the pseudoscalar, which is at least half of the nucleon mass: $E_{PS} > m_N/2$ in the CM frame, while the lowest order χPT is exact only at the zero energy (soft pion) limit. Of course, the direct method also relies upon leading order chiral perturbation theory at an energy scale around $m_N/2$. This is clearly a source of systematic error. However, since the extrapolation required is over a much shorter distance, it may be expected that the systematic error is smaller than that for the indirect method.

The indirect method requires the calculation of only a few two-point functions on the lattice. The direct method is superior to the indirect method since for the former there is no need to assume any parameter in the chiral Lagrangian to be in any particular range of values. Also, as mentioned, the former has less reliance on χPT. The coefficients are determined by the fit to the lattice results obtained for each decay process independently. The practical problem of the direct method is that it is typically an order of magnitude more demanding in computation than the indirect method for a similar statistical accuracy. This is because, for the direct method, many types (momenta, masses, and sources) of quark propagators must be solved and a larger temporal lattice size is needed to accommodate the three-point functions.

C. Lattice calculation setup

We give here brief details of the aspects of the lattice calculation which are common in the following sections. More detail will be provided in each section.

We use the domain-wall fermion (DWF) [35–37] action for quarks. At the expense of an additional fifth dimension, the DWF formulation preserves the flavor and chiral symmetries of continuum QCD at finite lattice spacing [38]. There are two main reasons to use a formulation with good chiral properties:

(1) Because of chiral symmetry, mixing between operators in different chiral multiplets is prohibited. As will be explained subsequently, for the particular case of interest this implies that the operators are renormalized multiplicatively, as in continuum QCD. Hence, simple and clean handling of the operator renormalization is possible.

(2) In lattice gauge simulations, one of the most important sources of systematic error is due to finite lattice spacing, a. Chiral symmetry disallows $O(a)$ scaling violations for both on- and off-shell Greens functions, which will participate in our estimate of the nucleon-decay matrix elements. As such, it suggests a mild dependence of any observables on a. Indeed, DWF has shown good scaling behavior in various hadronic quantities [39–43]. An important consequence of the fact that the propagator is off-shell improved is that nonperturbative renormalization becomes much simpler, allowing for the possibility of a significant reduction in systematic error.

For a fifth dimension of finite extent, there is still some explicit breaking of chiral symmetry by the DWF action. However, it may be hoped that such breaking is small enough for computationally reasonable extents of the fifth dimension so that it may be either ignored or treated as a small correction. Indeed, as it will be shown later, mixing of the operators is absent to a high degree of accuracy with a finite, affordable size of the fifth dimension.

A convenient quantity to parametrize the size of the explicit chiral symmetry breaking is the residual mass m_{res}, which acts as an additive renormalization to the fermion mass m_f, and is defined by considering the Ward-Takahashi (WT) identity [37],

$$\langle \mathcal{A}^a_\mu(x) J^b_5(0) \rangle = 2m_f \langle J^a_5(x) J^b_5(0) \rangle + 2\langle J^a_{5q}(x) J^b_5(0) \rangle + i\langle \delta^a J^b_5(0) \rangle, \tag{25}$$

$$m_{\mathrm{res}} = \frac{\sum_{\vec{x}} \langle J^a_{5q}(\vec{x}, t) J^b_5(0) \rangle}{\sum_{\vec{x}} \langle J^a_5(\vec{x}, t) J^b_5(0) \rangle}, \qquad (t \gg 1), \tag{26}$$

where $\mathcal{A}^a_\mu$ is the flavor-nonsinglet axial current defined using the bulk 5d fermion field and is a point-split bilinear operator in the 4d sense. J_5 is the pseudoscalar field constructed from the 4d quarks which are defined from the 5d domain-wall fermion field by taking the values at both walls, $s = 0, L_s - 1$ (L_s is the size of the fifth dimension). J_{5q} is similar to J_5, but is defined with the fermion field located at the midpoints ($s = L_s/2 - 1, L_s/2$) of the fifth dimension. The definition of m_{res} is such that the WT identity takes the same form as that in the continuum, with a shifted mass of $m_f + m_{\mathrm{res}}$ [44]. Hence, $\mathcal{A}^a_\mu$ is often called the "conserved axial current." Note that, by the WT

identity, at $m_f = -m_{\rm res}$ the pion mass must vanish, $m_\pi^2 \to 0$ as $(m_f + m_{\rm res}) \to 0$. For further details of our conventions and notation, see [40].

It has been demonstrated in quenched calculations that the chiral properties of DWF are improved on configurations generated by improved gauge actions [42,45]. In particular, the DBW2 gauge action [46,47] is superior in the smallness of $m_{\rm res}$ at a given L_s [42]. We use this DBW2 gauge action for both quenched and dynamical fermion simulations. The drawback of using the DBW2 action is that the sampling of different topological sectors becomes harder for finer lattices, which has already been observed for $a \simeq 0.1$ fm [42]. The main quenched calculation in this study uses a coarser lattice, with $a = 0.15$ fm, where the sampling problem is absent. We also use an ensemble with $a = 0.1$ fm, where we are able to overcome the sampling problem by setting a larger separation in Monte Carlo time.

Because of the smallness of the explicit chiral symmetry breaking, $\mathcal{A}_\mu^a$ can be treated as a (partially) conserved current to a good precision. As such, one can calculate the renormalization of the naive local (nonconserved) axial vector current, A_μ^a, by taking the ratio

$$Z_A \simeq \frac{\langle \sum_{\vec{x}} \mathcal{A}_\mu^a(\vec{x}, t) J_5^a(0) \rangle}{\langle \sum_{\vec{x}} A_\mu^a(\vec{x}, t) J_5^a(0) \rangle}, \qquad (t \gg 1). \tag{27}$$

Here, due to the point-split nature of $\mathcal{A}_\mu^a(x)$, a linear combination of the displaced operators should be used to get rid of the $O(a)$ error and to reduce the $O(a^2)$ error [48]. Precise details of this technique can be found in [40,42]. The axial current renormalization calculated in this way is used as a building block of our nonperturbative renormalization of the nucleon-decay operators.

Table I summarizes the simulation parameters. Our main effort is devoted to the quenched simulation ($N_f = 0$) at $a = 0.15$ fm, where we perform both direct and indirect measurements of the nucleon-decay matrix elements. A finer lattice with $N_f = 0$ will be used to discuss the finite lattice spacing and volume effects. An investigation using a dynamical fermion for the indirect calculation of the nucleon-decay matrix element has also been performed to evaluate the quenching effect.

III. OPERATOR RENORMALIZATION

In order to relate matrix elements obtained with the bare lattice operator to the continuum counterpart in a given renormalization scheme, one needs a well prescribed way to renormalize the lattice operator. In the literature, perturbation theory has been used for the renormalization of the nucleon-decay operators on the lattice. However, lattice perturbation theory suffers from bad convergence, primarily due to the tadpole contribution. Mean field improved perturbation theory [49] works much better. However, when compared to nonperturbative extractions, there are some operators for which it is inaccurate. Moreover, the definition is ambiguous. To be precise, there are several ways to select the mean field factor, and the resulting renormalization factor sometimes depends on the choice, and it is indeed the case for the nucleon-decay operator for DWF [25]. These problems are naively expected to disappear in the continuum limit. However, it is preferable to avoid such an ambiguity.

Nonperturbative renormalization (NPR) solves these problems. In this work we employ the nonperturbative, momentum (MOM)-scheme, renormalization technique of the Rome-Southampton group [50], which has previously been successfully used in conjunction with DWF [51,52] in the context of the renormalization of the flavor nonsinglet quark bilinear operators and four-quark operators relevant to kaon physics. Since the MOM scheme can be applied to any regularization, it is also referred to as the regularization independent (RI/MOM) scheme. Our approach in this work is to use NPR on the lattice to extract the renormalization factors defined at some scale in the MOM scheme, and then match the MOM scheme to the $\overline{\rm MS}$ scheme, which is more commonly used for the calculation of Wilson coefficients, using continuum perturbation theory. The renormalized operators are regularization independent up to the discretization error for the lattice calculation, e.g. $O(a)$ for Wilson, $O(a^2)$ for DWF, and up to the truncation error in continuum perturbation theory. Since we are relying—in part—on continuum perturbation theory, we must work at a momentum scale for which it is applicable, and so we need this renormalization scale to be much greater than $\Lambda_{\rm QCD}$. This may cause a problem

TABLE I. Domain-wall fermion simulation parameters for quenched ($N_f = 0$) and unquenched ($N_f = 2$) runs with DBW2 gauge action. Lattice spacing a indicates the approximate value with the ρ mass input at the chiral limit. The unrenormalized, approximate value of $m_{\rm res}$ is presented in physical units. A more detailed value will be shown in the later sections. "# configs." shows the number of configurations analyzed in either matrix element (ME) or NPR calculations. Unquenched simulation takes three sets of degenerate masses.

N_f	a (fm)	$6/g^2$	$L_\sigma^3 \times L_\tau$	L_s	M_5	$m_{\rm res}$ (MeV)	# configs. (ME)	# configs. (NPR)
0	**0.15**	**0.87**	$16^3 \times 32$	**12**	**1.8**	**1.3**	**100**	**51**
0	0.1	1.04	$16^3 \times 32$	16	1.7	0.04	400	55
2	0.12	0.8	$16^3 \times 32$	12	1.8	2.3	94×3	37–47

because the lattice discretization error grows as the momentum becomes larger. This is the well-known window problem: is it possible to have a region of momentum such that $\Lambda_{\rm QCD} \ll |p| \ll \pi/a$? We will give an estimate of the systematic error due to the window problem later.

The anomalous dimension of the nucleon-decay operator has been calculated up to two loops [53] using NDR in QCD. We use this result both in the scheme-matching calculation and to factorize the proper scale dependence of the NPR-MOM renormalization factor. In general, scheme dependence appears at the next-to-leading order (NLO), and so the one-loop matching factor which relates the MOM scheme to the $\overline{\rm MS}$, NDR scheme is needed for the complete NLO treatment of the operator renormalization. The result for this will be presented in Appendix C.

A. Operator mixing

Given the good chiral symmetry of DWF, the mixing of the operators with different chirality is expected to be suppressed. However, it is instructive to first enumerate the allowed mixings if chiral symmetry is not assumed. Since this discussion uses only the rotational, parity, and vector flavor symmetry of lattice QCD, it also gives the operator mixing structure for Wilson fermions.

It is convenient to introduce the operator basis which mimics those commonly used for the four-Fermi operators in the weak effective Hamiltonian. All the operators can be written in the form

$$\mathcal{O}^{\Gamma\Gamma'}_{uds} = \epsilon^{ijk}(u^{iT}C\Gamma d^j)\Gamma' s^k, \tag{28}$$

which should be the Lorentz spinor; thus all suffixes other than the single spin index must be contracted. Here, again u, d, and s are not necessarily labeling the real flavors. With a notation, $S = 1$, $P = \gamma_5$, $V = \gamma_\mu$, $A = \gamma_\mu\gamma_5$, $T = \sigma_{\mu\nu} = \frac{1}{2}\{\gamma_\mu, \gamma_\nu\}$, $\tilde{T} = \gamma_5\sigma_{\mu\nu}$, we have $\Gamma\Gamma' = SS$, PP, VV, AA, TT for the negative parity ($\mathcal{P}^-$) operators, and SP, PS, VA, AV, $T\tilde{T}$ for the positive parity ($\mathcal{P}^+$) operators [54]. There is another global symmetry which is useful in classifying these operators: switching ($\mathcal{S}$) u and d is a symmetry of the Lagrangian if they are degenerate in mass. Under a switching transformation, an operator comes back to itself with possible change of sign depending on Γ that connects the spin indices of u and d. Recalling $(C\Gamma)^T = -C\Gamma$ for $\Gamma = S$, P, A ($\mathcal{S}^-$) and $(C\Gamma)^T = +C\Gamma$ for $\Gamma = V$, T ($\mathcal{S}^+$), we have four different operator groups as shown in Table II. Operators in different blocks do not mix with each other.

TABLE II. Classification of the nucleon-decay three-quark operator $\mathcal{O}^{\Gamma\Gamma'}_{uds}$ by parity ($\mathcal{P}$) and switching ($\mathcal{S}$) ($u \leftrightarrow d$).

	$\mathcal{S}^-$			$\mathcal{S}^+$	
$\mathcal{P}^-$	SS	PP	AA	VV	TT
$\mathcal{P}^+$	SP	PS	$-AV$	$-VA$	$T\tilde{T}$

These operators have the following properties:

(1) There is a trivial relation between operators with different parity in the same column in Table II: $\mathcal{O}(\mathcal{P}^+) = \gamma_5\mathcal{O}(\mathcal{P}^-)$. This means that there is a one to one mapping between the parity negative and parity positive operators such that the renormalization matrices are identical.

(2) The five operators in $\mathcal{O}(\mathcal{P}^-)$ form a complete set of operators made of u, d, and s with any ordering. This follows from the fact that any such operator can be rewritten, by Fierz transformation, as a linear combination of the operators $\mathcal{O}^{\Gamma\Gamma'}_{uds}$.

(3) As our target operator is $\Gamma\Gamma' = P_{R/L}P_L$ [Eqs. (5) and (7)], we may neglect the $\mathcal{S}^+$ sector from possible mixing candidates. Then, for each parity (chirality), we need to consider only three operators for mixing.

(4) Operators of the type udu are renormalized in the same way as uds. A simple way to see this is to note that the calculation of these renormalization factors using the Rome-Southampton NPR method is identical. This will be shown below.

From now on, we can concentrate on the $\mathcal{S}^-$ sector. Our renormalization convention is

$$\mathcal{O}^{\,a}_{\rm ren} = Z^{ab}_{\rm ND}\mathcal{O}^b_{\rm latt}, \tag{29}$$

where a and b stand for possible $\Gamma\Gamma' = SS$, PP, AA for $\mathcal{P}^-$. $Z^{ab}_{\rm ND}$ is a 3×3 renormalization matrix. As mentioned above, an identical matrix applies for $\mathcal{P}^+$ operators, SP, PS, and AV. The chirality basis, which is more convenient to match the lattice operators with those used in the principal matrix elements, is made of the following three operators,

$$LL = \tfrac{1}{4}(SS + PP) - \tfrac{1}{4}(SP + PS), \tag{30}$$

$$RL = \tfrac{1}{4}(SS - PP) - \tfrac{1}{4}(SP - PS), \tag{31}$$

$$A(LV) = \tfrac{1}{2}AA - \tfrac{1}{2}(-AV). \tag{32}$$

The renormalization matrix transforms under this basis change as

$$Z^{\rm chiral}_{\rm ND} = TZ^{\rm parity}_{\rm ND}T^{-1}, \tag{33}$$

$$T = \begin{pmatrix} 1/4 & 1/4 & 0 \\ 1/4 & -1/4 & 0 \\ 0 & 0 & 1/2 \end{pmatrix}, \tag{34}$$

where $Z^{\rm chiral}_{\rm ND}$ is for the basis operators LL, RL, $A(LV)$, while $Z^{\rm parity}_{\rm ND}$ is for SS, PP, AA. If there is no explicit chiral symmetry breaking by the action used, $Z^{\rm chiral}_{\rm ND}$ is a diagonal matrix.

Taking the above into consideration, we may contrast the situation when using Wilson and domain-wall fermions: In the Wilson fermion case, the lattice operator, for

example the LL operator, is renormalized at one loop [20,22] as

$$\mathcal{O}_{LL}^{\overline{\mathrm{MS}}}(\mu) = \left(1 + \frac{\alpha_s}{4\pi}[4\log(\mu a) + \Delta]\right)\mathcal{O}_{LL}^{\mathrm{latt}} + \frac{\alpha_s}{4\pi}(C_{RL}\mathcal{O}_{RL}^{\mathrm{latt}} + C_{A(LV)}\mathcal{O}_{A(LV)}^{\mathrm{latt}}), \quad (35)$$

where Δ, C_{RL}, and $C_{A(LV)}$ are scale independent constants. The discussion here has shown that these three operators in the rhs are all that would appear even to all orders of α_s. In the DWF case, the mixing between operators with different chirality (off-diagonal elements of $Z_{\mathrm{ND}}^{\mathrm{chiral}}$) is highly suppressed. This follows from the discussion which makes use of the low-energy effective theory of DWF [51]. Applying the same procedure, it can be simply shown that the off-diagonal elements are suppressed by a factor of m_{res}^2 [$< O(10^{-6})$ for all our parameters].

B. NPR formulation

To calculate the renormalization factors using the MOM scheme [50,51], we first calculate the Greens function of the particular operator in question with three external quark states in Landau gauge,

$$G^a(x_0, x_1, x_2, x_3) = \langle \mathcal{O}^a_{uds}(x_0)\bar{u}(x_1)\bar{d}(x_2)\bar{s}(x_3)\rangle. \quad (36)$$

We set $x_0 = 0$. A Fourier transformation is then performed on the three external quark legs with the same momentum p, which are then amputated to obtain the vertex function,

$$\Lambda^a(p^2) = \mathrm{F.T.}G^a(0, x_1, x_2, x_3)|_{\mathrm{Amp}}. \quad (37)$$

Writing the tensor indices explicitly, the renormalization condition of the MOM scheme reads

$$P^a_{ijk\beta\alpha\delta\gamma} \cdot Z_q^{-3/2} Z^{bc}_{\mathrm{ND}} \Lambda^c_{ijk\alpha\beta\gamma\delta} = \delta^{ab}, \quad (38)$$

where Z_q is the quark wave function renormalization; i, j, k are color indices; and α, β and γ, δ are Dirac indices associated with Γ, Γ', respectively.

The projection matrix P^a is chosen such that Eq. (38) holds for the free field case with $Z_q = 1, Z^{ab}_{\mathrm{ND}} = \delta^{ab}$. Then,

$$P^{SS} = \frac{1}{96}\epsilon^{ijk}(C^{-1})^{\beta\alpha}\delta^{\delta\gamma}, \quad (39)$$

$$P^{PP} = \frac{1}{96}\epsilon^{ijk}(\gamma_5 C^{-1})^{\beta\alpha}\gamma_5^{\delta\gamma}, \quad (40)$$

$$P^{AA} = \frac{1}{384}\epsilon^{ijk}(\gamma_5\gamma_\mu C^{-1})^{\beta\alpha}(\gamma_5\gamma_\mu)^{\delta\gamma}. \quad (41)$$

To simplify the notation, we define the matrix M as

$$M^{ab} = \Lambda^a_{ijk\alpha\beta\gamma\delta} \cdot P^b_{ijk\beta\alpha\delta\gamma}, \quad (42)$$

which is equal to $Z_q^{3/2}(Z_{\mathrm{ND}}^{-1})$ up to systematic errors.

The treatment of Z_q needs care [51], as its definition naturally involves the derivative with respect to the momentum, and the lattice momentum cannot be continuous. Here we exploit the accurate determination of Z_A from the hadronic matrix element [Eq. (27)]. The bilinear vertex function of the local axial current Λ_A calculated in the MOM scheme yields Z_q/Z_A. Thus, the ratio $\Lambda_A^{3/2}/M^{aa}$ will give $Z_{\mathrm{ND}}/Z_A^{3/2}$. Z_{ND} is calculated with these two measurements without directly dealing with Z_q.

As Z_A has no scale dependence in the continuum, it must not have scale dependence except for that brought by the discretization error [which starts at $O(p^2a^2)$] at the finite lattice spacing. The ratio $Z_{\mathrm{ND}}/Z_A^{3/2}$ then has the same scale dependence as the nucleon-decay operator up to $O(p^2a^2)$ scaling violations.

C. Scheme matching and renormalization-group running

As it is clear in the above discussion, we need to know the scale dependence of the renormalized nucleon-decay operator to separate it out from the potential lattice artifacts. Our goal is to quote values for the matrix elements of interest in the $\overline{\mathrm{MS}}$, NDR scheme at some scale, μ,

$$\mathcal{O}^{\overline{\mathrm{MS}}}(\mu) = U^{\overline{\mathrm{MS}}\leftarrow\mathrm{latt}}(\mu)\mathcal{O}^{\mathrm{latt}}, \quad (43)$$

where $U^{\overline{\mathrm{MS}}\leftarrow\mathrm{latt}}(\mu)$ is the renormalization factor needed. We are using a two-step renormalization procedure: first renormalize with the MOM scheme at scale p, and then match with the $\overline{\mathrm{MS}}$ scheme at μ. This leads to the equation

$$U^{\overline{\mathrm{MS}}\leftarrow\mathrm{latt}}(\mu) = U^{\overline{\mathrm{MS}}}(\mu; p)\frac{Z^{\overline{\mathrm{MS}}}(p)}{Z^{\mathrm{MOM}}_{\mathrm{cont}}(p)}Z^{\mathrm{MOM}}_{\mathrm{latt}}(p). \quad (44)$$

The $Z^{\mathrm{MOM}}_{\mathrm{cont}}$ and $Z^{\mathrm{MOM}}_{\mathrm{latt}}$ are MOM-scheme factors calculated using continuum perturbation theory and NPR on the lattice, respectively. $Z^{\overline{\mathrm{MS}}}(p)$ is the continuum $\overline{\mathrm{MS}}$ renormalization factor; $U^{\overline{\mathrm{MS}}}(\mu; p)$ is the renormalization group evolution factor from scale p to μ in $\overline{\mathrm{MS}}$. $Z^{\overline{\mathrm{MS}}}(p)/Z^{\mathrm{MOM}}_{\mathrm{cont}}(p)$ is the matching factor from the $\overline{\mathrm{MS}}$ scheme to the MOM scheme at scale p.

The anomalous dimension of the nucleon-decay operator, which enters $U^{\overline{\mathrm{MS}}}(\mu; p)$, has been calculated up to two loops in the $\overline{\mathrm{MS}}$, NDR scheme [53]. The anomalous dimension reads

$$\gamma = \gamma_0\frac{\alpha_s}{4\pi} + \gamma_1\left(\frac{\alpha_s}{4\pi}\right)^2, \quad (45)$$

$$\gamma_0 = -4, \qquad \gamma_1 = -\left(\frac{14}{3} + \frac{4}{9}N_f - 4\Delta\right), \quad (46)$$

where $\Delta = 0$ for the LL operator and $-10/3$ for the RL operator, and N_f is the number of active flavors [55]. The $\overline{\mathrm{MS}}$ evolution factor reads

$$U^{\overline{\mathrm{MS}}}(\mu;p)=\left[\frac{\alpha_s(\mu)}{\alpha_s(p)}\right]^{\gamma_0/2\beta_0}\left[1+\left(\frac{\gamma_1}{2\beta_0}-\frac{\beta_1\gamma_0}{2\beta_0^2}\right)\times\frac{\alpha_s(\mu)-\alpha_s(p)}{4\pi}\right], \quad (47)$$

$$\beta_0=11-\frac{2}{3}N_f, \qquad \beta_1=102-\frac{22}{3}N_f. \quad (48)$$

The matching factor is calculated to one loop in continuum perturbation theory. The MOM-scheme calculation should be performed with the same kinematics and in the same gauge as that used on the lattice. Setting the momenta for the three external quark fields to be equal, and setting the mass to zero, the matching factor is obtained as

$$\frac{Z^{\overline{\mathrm{MS}}}}{Z^{\mathrm{MOM}}}=1+\frac{\alpha_s}{4\pi}\left[\frac{433}{180}-\frac{1123}{90}\ln 2+\xi\left(\frac{587}{180}-\frac{317}{90}\ln 2\right)\right], \quad (49)$$

where ξ is the gauge parameter and $\xi=0$ (Landau gauge) will be used. See Appendix C for the derivation. To match the NPR-MOM scheme to the $\overline{\mathrm{MS}}$ scheme with this formula, we need to take the chiral limit of the massive simulation data. As we will see, this can be done very precisely, as this mass dependence is extremely mild in the NPR data.

We use the two-loop running coupling $\alpha_s(\mu)$ with $\Lambda_{\overline{\mathrm{MS}}}$ obtained by Alpha Collaboration for quenched QCD [56], $\Lambda^{(0)}_{\overline{\mathrm{MS}}} r_0 = 0.602(48)$, where r_0 is the Sommer parameter defined with the static quark potential $V(r)$ as $r^2\frac{dV}{dr}=1.65$ [57]. The approximate value is $r_0=0.5$ fm from the potential models. As we set the scale by using the ρ meson, we use our measurements of r_0/a and $m_\rho a$ and combine with the experiment $m_\rho=0.77$ GeV to get the appropriate $\Lambda^{(0)}_{\overline{\mathrm{MS}}}$.

D. Results of the NPR

We present here the results of the NPR of nucleon-decay operators for quenched calculation, on configurations generated with the DBW2 gauge action at $a=0.15$ fm (see Table I). The NPR study employs four quark masses $m_f=0.025, 0.04, 0.055, 0.07$, where the largest roughly corresponds to the strange quark mass.

Figure 1 shows the SS and PP projections of the SS operator, $M^{SS,SS}$ and $M^{SS,PP}$ as a function of lattice momentum squared for all quark masses. Note that mass dependence is negligible.

Taking the chiral limit ($m_f \to -m_{\mathrm{res}}$) using a linear extrapolation and rearranging to the chirality basis, one obtains Fig. 2 for all the elements of M.

Most of the off-diagonal elements are less than 0.5% of the diagonal and consistent with zero for $(pa)^2>1.2$ within 2σ, while a few others still remain within 1% of the diagonal elements, and are thus negligible for our extraction [58]. As a result, the nucleon-decay operator $\mathcal{O}^{R/LL}=\epsilon^{ijk}(u^{iT}CP_{R/L}d^j)P_L s^k$ is renormalized multiplicatively for our domain-wall fermion simulation.

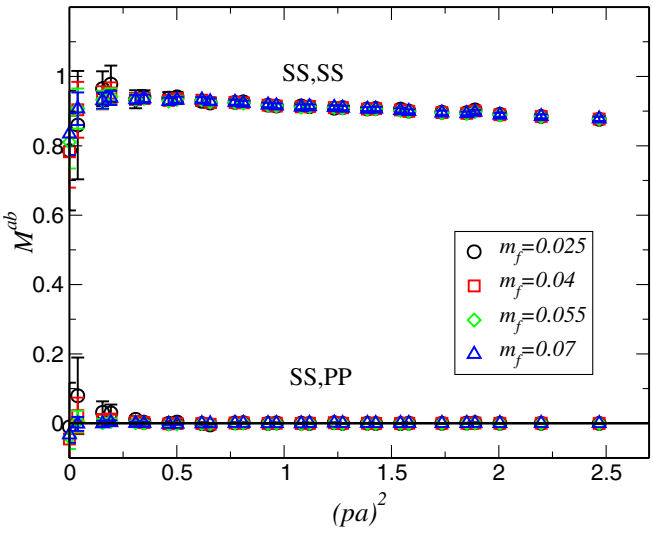

FIG. 1 (color online). SS and PP projections of the SS operator, $M^{SS,SS}$ and $M^{SS,PP}$, as a function of lattice momentum squared for each quark mass.

The next step is to obtain the total renormalization factor to relate the lattice operator to the $\overline{\mathrm{MS}}$, NDR operator, for which we need the value of Z_q. As mentioned previously, we extract this value by calculating Z_A/Z_q using the Rome-Southampton technique, and Z_A from hadronic correlators. For the former, we use the average of the vertex function of the local axial vector and vector current operators. The renormalization constants for these operators are equal in a theory in which chiral symmetry is only softly broken. This equality should also hold for the vertex functions at high energies. At low energies they can differ due

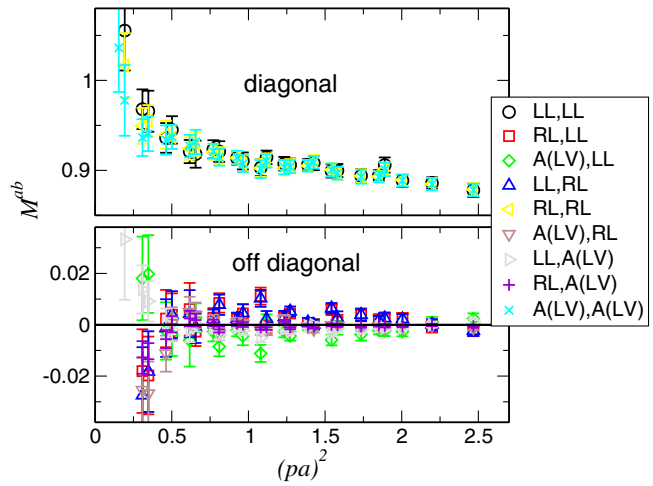

FIG. 2 (color online). Mixing matrix $M^{a,b}$ in the chirality basis at the chiral limit $m_f \to -m_{\mathrm{res}}$.

to the spontaneous breaking of chiral symmetry. Figure 3 shows the average and difference of the vertex function for A and V.

The nonzero difference at the value of the momenta which are accessible to our lattice calculations indicates that the window where the RI/MOM NPR can be safely applied is closing for the lattice spacing being used ($a = 0.15$ fm). This difference may be taken as a measure of the systematic error of the renormalization constant arising from the closing of the window. One sees up to 1.5% effect difference for $p^2 \geq 1.2$, which can be enhanced by the extrapolation, $(pa)^2 \to 0$ to 2%. We may estimate the systematic error of the nucleon-decay renormalization constants, from this source, as 3% considering the dimension of the operator.

Using the average of the axial and vector vertex functions, combined with the vertex function of the nucleon-decay operator, the diagonal elements of $Z_{\mathrm{ND}}^{\mathrm{MOM}}/Z_A^{3/2}$ can be calculated. This is shown in Fig. 4 for $\mathcal{O}^{LL}$ versus the renormalization scale squared. Using the results of the previously discussed matching and running calculations, the $\overline{\mathrm{MS}}$ renormalization factor [Eq. (44)] at fixed scale $\mu = 1/a$, which should thus be scale invariant, is shown as squares. This is, again, plotted versus the square of the scale at which the lattice, MOM-scheme, renormalization calculation was performed. We identify the remaining momentum dependence as $O(p^2a^2)$ discretization error. To extract the value at $(pa)^2 = 0$, the linear function in $(pa)^2$ is used to fit it in the region $1.2 < (pa)^2 < 2.5$, where the nonperturbative effect is expected to be small ($\lesssim 3\%$) and the higher order effect is negligible. Combining with

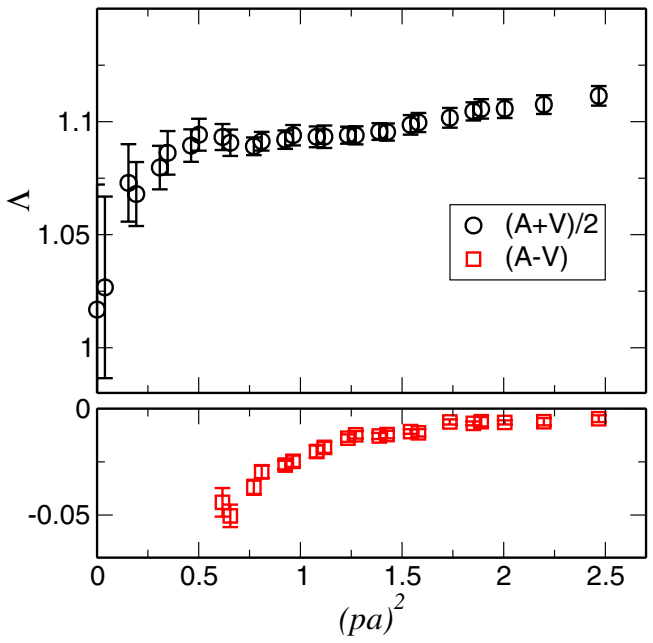

FIG. 3 (color online). Average and difference of the axial vector and vector vertex functions.

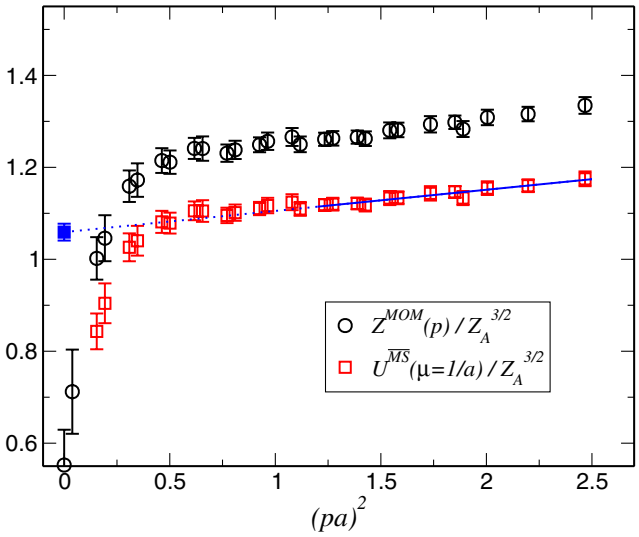

FIG. 4 (color online). Renormalization factor of the nucleon-decay operator ($\mathcal{O}_{LL}$) normalized by the axial current renormalization constant Z_A, for (a) (circle) the MOM scheme $Z_{\mathrm{latt}}^{\mathrm{MOM}}(p)/Z_A^{3/2}$ as a function of the renormalization scale p^2 and for (b) (square) the $\overline{\mathrm{MS}}$ scheme $U^{\overline{\mathrm{MS}}\leftarrow\mathrm{latt}}(\mu = 1/a)/Z_A^{3/2}$ [Eq. (43)] as a function of the MOM $\to$ $\overline{\mathrm{MS}}$ matching scale p^2.

the axial current renormalization (Table III) obtained with Eq. (27), and running from $\mu = 1/a$ to 2 GeV by Eq. (47), we get

$$U^{\overline{\mathrm{MS}}\leftarrow\mathrm{latt}}(2\ \mathrm{GeV}) = \begin{cases} 0.751(13)(45) & \text{for } \mathcal{O}^{LL}, \\ 0.755(15)(45) & \text{for } \mathcal{O}^{RL}, \end{cases} \tag{50}$$

where the value for $\mathcal{O}^{RL}$ has similarly been calculated. The first set of parentheses show the statistical error. The systematic error in the second set of parentheses involves two parts: one is from the window problem, which we already have estimated as 3%. The other is the perturbation theory error arising from truncating the higher order terms, which are of the order of α_s^2. We take $\alpha_s^2(p) \simeq 0.05$ at the smallest matching momentum $(pa)^2 = 1.2$ as the relative systematic error [59]. Thus, the total systematic error of the NPR is 6%.

We apply the same procedure to the $a = 0.1$ fm DBW2 lattices and get

$$U^{\overline{\mathrm{MS}}\leftarrow\mathrm{latt}}(2\ \mathrm{GeV}) = 0.805(9)(32) \tag{51}$$

for both $\mathcal{O}^{LL}$ and $\mathcal{O}^{RL}$. The systematic error from the window problem is negligible. The perturbation theory error is 4%, which is counted as the total systematic error for the renormalization factor.

IV. MATRIX ELEMENTS

In this section the details of the matrix element calculation in the quenched approximation are given.

TABLE III. The residual mass $m_{\rm res}$, axial current renormalization constant Z_A, hadron masses from the box source propagator, and pion decay constant f_π from the pseudoscalar two-point function with a gauge unfixed wall source propagator for $6/g^2 = 0.87$ ($a = 0.15$ fm) quenched domain-wall fermions. The nucleon-decay low-energy parameters α and β with bare operators are shown as well. Chiral extrapolation by an uncorrelated linear fit in m_f within the "range" of m_f is performed to get the "chiral limit," which is defined as $m_f \to -m_{\rm res}$, except for $m_f \to 0$, to get the chiral limit of $m_{\rm res}$ itself. For m_π, squared values are fitted and the "chiral limit" shows the square root of extrapolated m_π^2. All dimension-full quantities are in lattice units. Errors are by jackknife.

m_f	$m_{\rm res}(\times 10^{-3})$	Z_A	m_π	m_ρ	m_N	f_π	$\alpha(\times 10^{-3})$	$\beta(\times 10^{-3})$
0.02	1.171(29)	0.78405(38)	0.3060(25)	0.637(16)	0.858(17)	0.1107(9)	−6.85(66)	7.56(76)
0.04	1.076(25)	0.78770(28)	0.4172(22)	0.6866(69)	0.9698(83)	0.1205(9)	−7.54(46)	7.61(44)
0.06	1.005(22)	0.79173(23)	0.5066(20)	0.7352(42)	1.0722(62)	0.1290(9)	−8.28(42)	8.27(39)
0.08	0.955(21)	0.79609(21)	0.5849(18)	0.7829(32)	1.1651(52)	0.1368(9)	−9.05(42)	9.02(40)
chiral limit	1.248(34)	0.77983(46)	0.083(11)	0.587(12)	0.751(19)	0.1012(10)	−6.03(71)	6.57(76)
range	0.02–0.06	0.02–0.06	0.02–0.06	0.02–0.08	0.02–0.06	0.02–0.06	0.02–0.08	0.02–0.08
χ^2/dof	0.14(44)/1	0.29(18)/1	0.22(15)/1	0.01(16)/2	0.13(29)/1	0.31(19)/1	0.005(51)/2	0.49(60)/2

A. Parameters and lattice scale

The matrix elements and related hadron spectrum are calculated on the quenched DBW2 configurations with lattice spacing $a = 0.15$ fm (see Table I). The 100 configurations used are separated by 200 iterations of four overrelaxation steps and one heatbath step. The quark masses are $m_f = 0.02, 0.04, 0.06, 0.08$. The strange quark mass point is approximately between the largest two masses used. We use quark propagators with an antiperiodic boundary condition in the temporal direction to measure Z_A, $m_{\rm res}$. For all the other quantities, we average two quark propagators: one with periodic and the other with antiperiodic boundary conditions in the temporal direction. In this way we effectively double the temporal size to 64, for which we may safely neglect the effects of the hadrons moving around the temporal boundary in the three-point function measurements.

Table III shows the π, ρ, and nucleon masses, $m_{\rm res}$, local axial current renormalization Z_A, and pion decay constant f_π from the pseudoscalar two-point function, all calculated with the degenerate quarks. Nongaugefixed wall sources [60] are used for f_π. The other quantities use a quark source fixed into Coulomb gauge and uniformly distributed in a spatial cubic box, whose size is fixed to be 8^3 to optimize the nucleon signal. The hadron masses are obtained by the standard two-parameter correlated fit to the two-point functions. $m_{\rm res}$ and Z_A are calculated by the ratio method, Eqs. (26) and (27). $m_{\rm res}$ extrapolated to $m_f = 0$ is used as the chiral limit point $m_f \to -m_{\rm res}$. In the table, chiral limit values from a linear fit in m_f are also shown. For pion mass, m_π^2 is also fit to the linear function of m_f. The lower bound of the fitting range is always the smallest mass, $m_f = 0.02$. For all measurements except for the ρ meson mass, we exclude largest mass $m_f = 0.08$ from the chiral fit to stay in the region of good linearity. Taking the experimental ρ mass input (0.77 GeV) and comparing to the chiral limit, the lattice cutoff is determined,

$$a^{-1} = 1.312(27)\ \text{GeV}. \tag{52}$$

If we took $f_\pi = 0.131$ GeV as an input, we would obtain $a^{-1} = 1.294(13)$ GeV which is consistent with the ρ input. For the nucleon mass $m_N = 0.938$ GeV as an input, $a^{-1} = 1.249(32)$ GeV. This scale ambiguity (5%) between ρ and nucleon input, likely predominated by a combination of extrapolation and quenching errors, will be used as the systematic error of the matrix elements in physical units. Using $a = 0.150(3)$ fm from ρ input, the spatial lattice size is obtained as $L_\sigma = 2.4$ fm, which should be large enough for a nucleon with our mass range [61], and can accommodate momentum small enough to directly reach the physical kinematics region of the nucleon to pion decay.

The simple linear extrapolation of the pion mass to the chiral limit gives a nonzero value. Rather than evidence of numerically significant chiral symmetry breaking which is not already taken into account by the residual mass, we take this as a sign of nonanalyticity at small mass. In fact, fitting using a formula including quenched chiral logarithms suggested by the quenched chiral perturbation theory (QχPT) leads to a fit with reasonable χ^2 under the constraint that m_π vanishes at $m_f = -m_{\rm res}$. We use $m_f = -m_{\rm res}$ as the chiral limit of DWF, thus as the physical u, d masses in our approximation, throughout the paper. Apart from the pion in the chiral limit, we use leading linear dependence on the quark mass to interpolate or extrapolate to the physical points for all the quantities.

The strange mass point $m_f^{(s)}$ is obtained as $m_\pi^2(m_f^{(s)}, m_f^{(s)}) = 2m_K^2$ using the linear fit results to interpolate, where $m_K = 0.497$ GeV,

$$m_f^{(s)} = 0.0675(30). \tag{53}$$

This will be used to interpolate the mass of $\bar{s}$ in the kaon for the form factors.

B. Hadronic matrix elements

The low-energy parameters α and β [Eqs. (20) and (21)] of the nucleon-decay chiral Lagrangian are calculated through the ratio of the two-point functions,

$$R_{\alpha/\beta}(t) = \frac{\sum_{\vec{x}} \langle \mathcal{O}^{R/LL}_{udu}(\vec{x}, t) \bar{J}_p(t_0) \rangle}{\sum_{\vec{x}} \langle J_p(\vec{x}, t) \bar{J}_p(t_0) \rangle} \sqrt{Z_p}. \tag{54}$$

A quark propagator with a cubic box source of 8^3 volume at $t = t_0$ is used for both two-point functions in the numerator and the denominator. The factor $\sqrt{Z_p}$ is the overlap of the proton interpolating field to the normalized proton state,

$$\langle 0 | J_p(\vec{0}, 0) | p \rangle = \sqrt{Z_p} u_p, \tag{55}$$

for the local proton interpolating field $J_p(x)$ and the proton spinor with the standard relativistic normalization [see Appendix A, Eq. (A2)]. Z_p could be measured via the amplitude of the single exponential fit to the point-point proton two-point function. However, this fit is often problematic. Instead, we estimate it through the ratio of the proton two-point functions with point and box source propagators, both with point sink. The asymptotic value of the ratio gives the ratio of the amplitudes with the point-pion and box-point propagators. Given the amplitude of the box-point propagator, which is more accurate than that with the point-point, Z_p is finally obtained.

Figure 5 shows the ratio $R_\alpha(t)$ [Eq. (54)] for $m_f = 0.04$ and 0.08. By fitting to a constant, $\alpha(m_f)$ is obtained. Figure 6 shows the fitted α at finite m_f, which is extrapolated with the linear function in m_f to the chiral limit [62]. Our estimate of the low-energy parameters with the operators renormalized at $\mu = 2$ GeV is

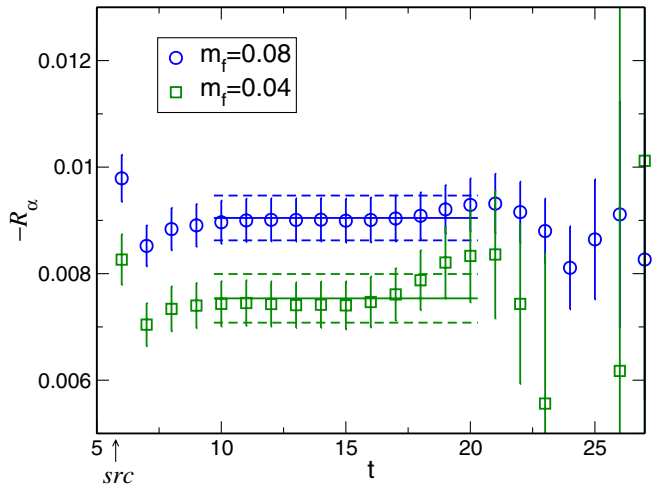

FIG. 5 (color online). The ratio $R_\alpha(t)$ [Eq. (54)] for the low-energy parameter α at $m_f = 0.04$ and 0.08 on quenched DBW2 configurations, shown against the operator position (t), where the proton source is located at $t_0 = 6$.

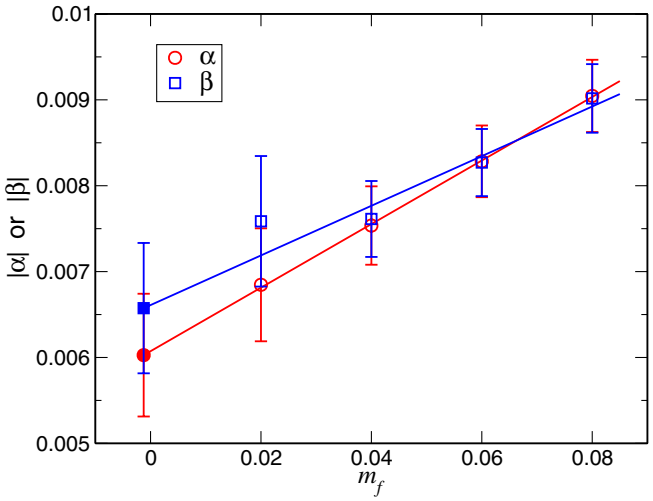

FIG. 6 (color online). $|\alpha|$ and $|\beta|$ obtained from the ratio $R_{\alpha/\beta}(t)$ as functions of m_f on quenched DBW2 configurations. Linear extrapolation is performed to get the values in the chiral limit ($m_f \to m_{\rm res}$). Values are in lattice units and are unrenormalized.

$$-\alpha = 0.0100(12)(14)(6)\ \text{GeV}^3, \tag{56}$$

$$\beta = 0.0108(13)(15)(7)\ \text{GeV}^3, \tag{57}$$

where the first set of parentheses shows the statistical error from the bare matrix element, the second is the systematic error from the scale ambiguity, and the third comes from the total error of the renormalization factor.

The direct method [22] amounts to calculating a ratio of the three- and two-point functions. For the proton to π case, the ratio is

$$R_3^{\vec{p}}(t) = \frac{\sum_{\vec{x}_1, \vec{x}} e^{i\vec{p}\cdot(\vec{x}_1 - \vec{x})} \langle J_\pi(\vec{x}_1, t_1) \mathcal{O}^{R/LL}(\vec{x}, t) \bar{J}_p(t_0) \rangle}{\sum_{\vec{x}_1, \vec{x}} e^{i\vec{p}\cdot(\vec{x}_1 - \vec{x})} \langle J_\pi(\vec{x}_1, t_1) J^\dagger_\pi(\vec{x}, t) \rangle \cdot \sum_{\vec{x}} \langle J_p(\vec{x}, t) \bar{J}_p(t_0) \rangle} \times \sqrt{Z_\pi Z_p} L_\sigma^3, \tag{58}$$

with Z_π being the overlap of the pion interpolating field to the normalized pion state,

$$\langle \pi | J^\dagger_\pi(0) | 0 \rangle = \sqrt{Z_\pi}. \tag{59}$$

Again, the proton interpolating field at $t = t_0$ is made of quark fields distributed uniformly in an 8^3 box. The associated quark propagators are solved with $m_f = m_1$. In the three-point function, as depicted in Fig. 7, two quarks from the nucleon source are annihilated by the operator at $t = t$. The other is a spectator, which is annihilated by the pion interpolating field at $t = t_1$. To interpolate the pion with momentum, a quark propagator is solved sequentially with $m_f = m_2$ and with the source equated with the spectator

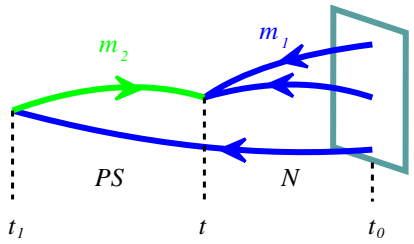

FIG. 7 (color online). Diagram of the quark line contraction of the nucleon-decay ($N \to PS$) three-point function.

quark propagator at $t = t_1$ with the momentum projection $e^{i\vec{p}\cdot\vec{x}}$, which acts as an injection of the momentum $\vec{p}$. The resulting sequential quark propagator is finally contracted as the third quark of the operator at $t = t$. The momentum $-\vec{p}$ is injected into the operator.

The pion two-point function in the denominator is made with the two quark propagators constructed using non-gaugefixed wall sources at $t = t_1$ and with mass m_1 or m_2. One source is always a zero momentum wall, while the other is made with the distribution of $e^{i\vec{p}\cdot\vec{x}}$, where the momentum $\vec{p}$ should be matched to the momentum injected into the sequential quark propagator in the numerator. Combining the two propagators of this type, the pseudoscalar operator at the t_1 time slice becomes a local operator after averaging over the gauge configurations, as the nonlocal terms vanish [60] by Elitzur's theorem [63]. The nongaugefixed source works well for the pseudoscalar operator and is superior to the local source in signal/noise ratio. At time t, the quark and the antiquark are annihilated by the local pion field $J^{\dagger}_{\pi}(x)$ with momentum injection.

We only work with masses satisfying $m_1 \leq m_2$, which is enough to extrapolate/interpolate to the pion $[(m_1, m_2) \to (-m_{\rm res}, -m_{\rm res})]$ or kaon $[(-m_{\rm res}, m_f^{(s)})]$ physical point. For extrapolation to physical kinematics, $\vec{p}L_\sigma/2\pi = (1, 0, 0)$ and (1,1,0) are used, where $L_\sigma = 16$ is the spatial size. Zero momentum $\vec{p} = (0, 0, 0)$ data are taken only for $m_1 = m_2$ points to discuss the soft pion limit in Appendix B.

The matrix element is extracted by fitting the plateau of the ratio as a function of the position of the operator t. Some care is needed to extract the relevant form factor W_0 [22]. The nucleon interpolating field also interpolates the parity partner of the nucleon, which has to be eliminated by the parity projector. Then, naively taking the trace of the ratio, we obtain

$$\mathrm{Tr}\left\{P_L[W_0 - i\not{q}W_q]\left(\frac{1+\gamma_4}{2}\right)\right\} = W_0 - iq_4 W_q. \quad (60)$$

The irrelevant form factor is calculated as

$$\mathrm{Tr}\left\{P_L[W_0 - i\not{q}W_q]\left(\frac{1+\gamma_4}{2}\right)i\gamma_j\right\} = q_j W_q, \quad (61)$$

where $q_j = -p_j$, the injected spatial momentum with negative sign. Combined with the calculated energy transfer $iq_4 = E_p - E_\pi$, W_0 is finally disentangled.

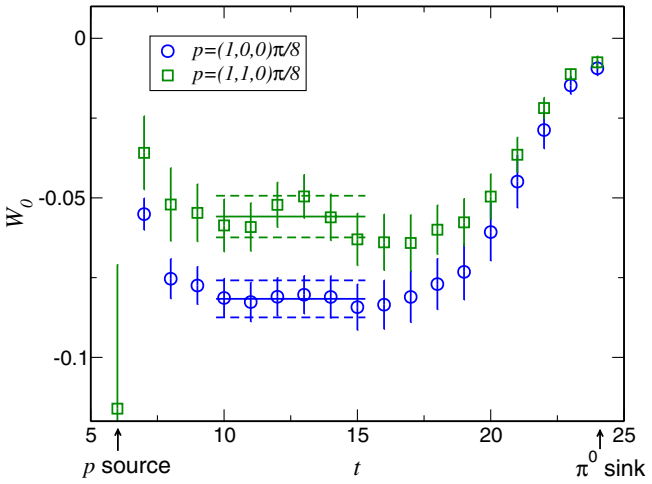

FIG. 8 (color online). Ratio, Eq. (58), for the relevant form factor W_0 of $\langle\pi^0|(ud)_R u_L|p\rangle$ with the bare operator and in lattice units at $m_f = 0.06$.

Figure 8 plots the W_0 part of the ratio, Eq. (58), as a function of t for $\langle\pi^0|(ud)_R u_L|p\rangle$ at $m_f = 0.06$. Fitting the plateau in the range $10 \leq t \leq 15$, which appears to be a reasonably good fitting range for all the processes and parameters, $W_0(m_f, q^2)$ is obtained and plotted in Fig. 9 as a function of $-q^2$. The results are given in lattice units and for the bare operator. The solid diamond shows the

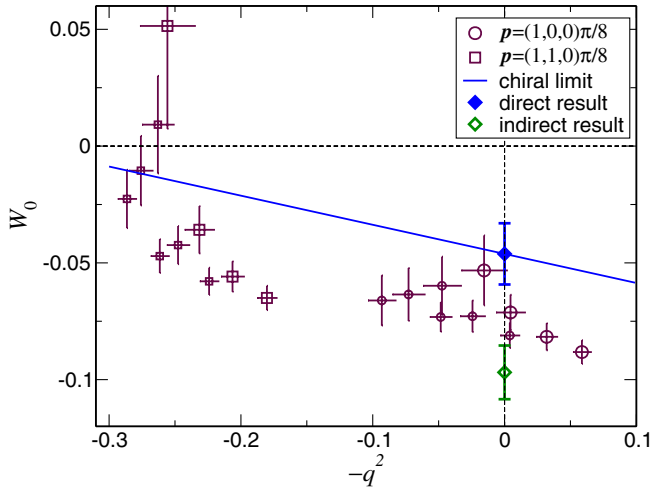

FIG. 9 (color online). Relevant form factor W_0 of $\langle\pi^0|(ud)_R u_L|p\rangle$ as a function of $-q^2$. Circles and squares are the measured data with the pion having the smallest and the second smallest momentum on the periodic lattice, respectively. Larger symbols show the degenerate mass points ($m_1 = m_2$), while the smaller indicate nondegenerate mass points ($m_1 \neq m_2$). The line shows the chiral limit obtained from the fit [Eq. (62)]. The solid diamond indicates the physical kinematics point $q^2 \to 0$. The open diamond is from the indirect method.

extrapolation to the physical point ($m_1 \to -m_{\rm res}$, $m_2 \to -m_{\rm res}$, $q^2 \to 0$), using [64]

$$W_0 = c_0 + c_1(m_1 + m_{\rm res}) + c_2(m_2 + m_{\rm res}) + c_3 q^2. \quad (62)$$

This formula is obtained using leading order χPT, expanded in q^2 and quark mass $m_q = m_f + m_{\rm res}$. Quark mass is naturally interpreted as m_{PS}^2, which has size similar to q^2 at the simulated points. The open diamonds are from the indirect method, Eq. (20), taking $f_\pi = 0.131$ GeV from experiment. Inputting f_π from our lattice measurement gives a consistent result. Since the operators are renormalized multiplicatively (see Sec. III), the results will be unchanged after renormalization up to an overall factor. The indirect calculation estimates W_0 to be larger by about a factor of 2 than the direct method. A similar disagreement is seen for the LL operator case, which is shown in Fig. 10. This difference, though large, is not surprising. At the physical kinematics point, where the pion momentum is large $|\vec{p}| = m_N/2 \simeq m_K$, one might expect LO χPT to lose its effectiveness. On the other hand, the soft pion limit should be described by LO χPT exactly. The discussion on this point is given in Appendix B.

The same analysis has been carried out for the other principal matrix elements. All the results for $W_0(m_1, m_2, q^2)$ are summarized in Tables VII, VIII, and IX in Appendix D. The fit results with Eq. (62) are listed in Table X. Figure 11 plots the final results of W_0 at the physical kinematics in physical units for the renormalized operator. The indirect method estimates the form factors to be larger than the direct method does for most of the cases. Note that, for several processes, the difference of the two estimates is significant.

Table IV shows the relevant form factors for all the possible matrix elements. This is the main result of this paper. We note that the total error is dominated by the statistical error of the matrix element.

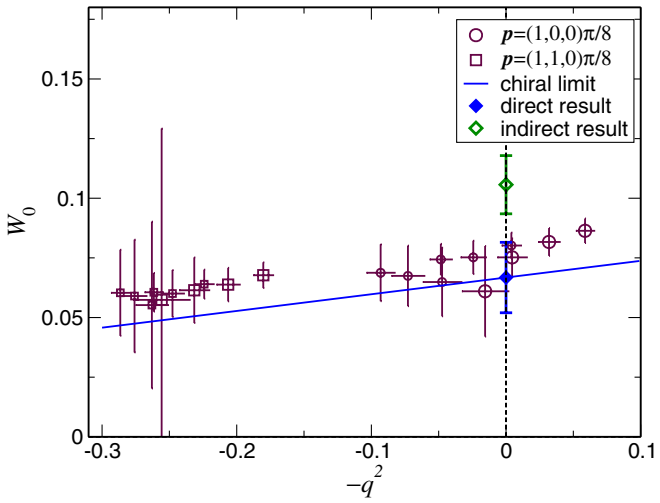

FIG. 10 (color online). Same as Fig. 9, but for $\langle \pi^0 | (ud)_L u_L | p \rangle$.

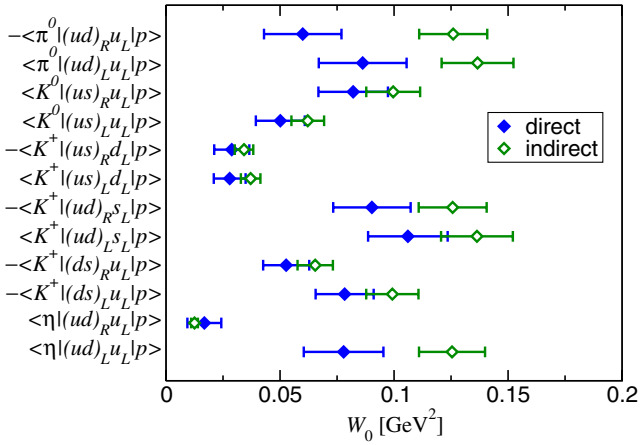

FIG. 11 (color online). Relevant form factors of all the principal matrix elements for nucleon decay with the quenched approximation. Operators are renormalized by the $\overline{\rm MS}$, NDR scheme at $\mu = 2$ GeV. The errors are statistical only.

The values of individual matrix elements are different from those obtained for $a^{-1} \simeq 2.3$ GeV with the Wilson fermion [22], while ratios of the matrix elements are similar. We expect our DWF results to be closer to the continuum limit, as discussed below.

C. Systematic errors

The major sources of systematic error for this calculation are as follows:

(1) finite lattice spacing a,
(2) finite system volume,
(3) chiral extrapolation,
(4) quenching effects.

Among these, 1 and 2 are relatively easier to address, and, as we will see below, there are reasons to believe they are small.

To evaluate the systematic errors 1 and 2, we compare quantities already shown with those obtained on the finer lattice spacing and smaller volume. We have used a $6/g^2 = 0.87$ lattice, where lattice spacing is $a = 0.15$ fm and 16^3 lattice volume corresponds to $(2.4\ \text{fm})^3$ box. The finer lattice parameter is a $6/g^2 = 1.04$, $a = 0.1$ fm, $(1.6\ \text{fm})^3$ box.

First, we compare the hadron masses in Table III with those obtained [42] on the finer lattice. Figure 12 shows the hadron masses normalized by r_0 [65] against the quark mass $r_0 Z_m(m_f + m_{\rm res})$ renormalized at $\mu = 2$ GeV in the $\overline{\rm MS}$, NDR scheme. The quark mass renormalization factors are taken from Ref. [66], where only the $L_s = 16$ case is studied. The difference of Z_m between $L_s = 12$, which has been used in this study, and $L_s = 16$ should be negligible. The error shown in the figure is statistical only.

At larger masses, hadrons are compact; hence the volume effect should be small. The consistency of the hadron masses at larger quark mass suggests the finite lattice

TABLE IV. The relevant form factors W_0 (GeV^2) for all the possible matrix elements [Eqs. (8)–(14)], with the operator renormalized at $\mu = 2$ GeV with the $\overline{\text{MS}}$, NDR scheme. The first error is the total error, which is obtained by adding in quadrature the statistical error of bare W_0 (second quoted error), the systematic error from the scale, and the total error of the renormalization factor. Note, again, that in the present calculation the flavor $SU(3)$ breaking effect of η is not taken into account.

Matrix element	*RL* or *LR* operator			*LL* or *RR* operator		
	W_0 (GeV^2)	Total error	Stat. error	W_0 (GeV^2)	Total error	Stat. error
$\langle\pi^0\|(ud)u\|p\rangle$, $\langle\pi^0\|(du)d\|n\rangle$	−0.060	0.018	0.017	0.086	0.022	0.019
$\langle\pi^+\|(ud)d\|p\rangle$, $-\langle\pi^+\|(du)u\|n\rangle$	−0.085	0.026	0.024	0.122	0.030	0.027
$\langle K^0\|(us)u\|p\rangle$, $-\langle K^+\|(ds)d\|n\rangle$	0.082	0.018	0.015	0.050	0.012	0.011
$\langle K^+\|(us)d\|p\rangle$, $-\langle K^0\|(ds)u\|n\rangle$	−0.029	0.008	0.008	0.028	0.008	0.007
$\langle K^+\|(ud)s\|p\rangle$, $-\langle K^0\|(du)s\|n\rangle$	−0.090	0.020	0.017	0.106	0.021	0.017
$\langle K^+\|(ds)u\|p\rangle$, $-\langle K^0\|(us)d\|n\rangle$	−0.053	0.012	0.010	−0.078	0.015	0.013
$\langle\eta\|(ud)u\|p\rangle$, $-\langle\eta\|(du)d\|n\rangle$	0.017	0.008	0.007	0.078	0.020	0.017

spacing error is negligible within our accuracy. Furthermore, the consistency is seen all the way down to the smallest mass of $a = 0.15$ fm. This suggests that the volume effect is also negligible in the mass range studied.

More direct evidence that the systematic errors 1 and 2 are small is seen in Fig. 13, where the difference of the two low-energy parameters $|\alpha - \beta|$ is shown in the same way as Fig. 12. We have used the relation of the proton interpolating field [Eq. (A9)] to a nucleon-decay operator,

$$J_p = (\mathcal{O}^{RL}_{udu} - \mathcal{O}^{LL}_{udu}) + (\mathcal{O}^{RR}_{udu} - \mathcal{O}^{LR}_{udu}), \tag{63}$$

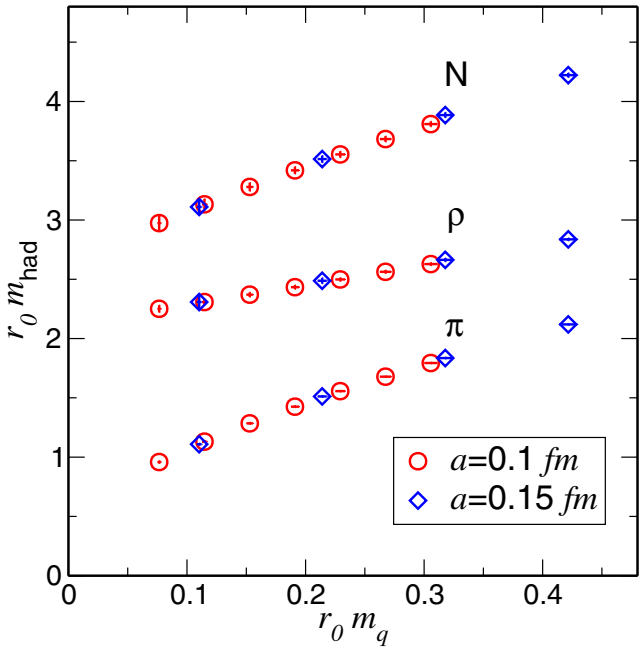

FIG. 12 (color online). Hadron masses as a function of quark mass renormalized at $\mu = 2$ GeV with the $\overline{\text{MS}}$, NDR scheme. Both axes are normalized by r_0. Both lattices have $16^3 \times 32$ volume. Larger lattice spacing $a = 0.15$ fm has been used for the nucleon-decay matrix element. Volume and lattice spacing effects are negligible.

and hence

$$\langle 0|J_p|p\rangle = (\alpha - \beta)u_p. \tag{64}$$

Thus, $\alpha - \beta$ can be extracted from the ordinary nucleon two-point function $\langle J_p(x)\bar{J}_p(0)\rangle$ as well. Since the renormalization factors of the nucleon-decay operators of different chirality are the same within the error, their average may be used to renormalize J_p to get $\alpha - \beta$. For the finer lattice results, we have reused the $a = 0.1$ fm data for the spectrum study [42]. The same arguments as the hadron masses lead to the observation that the systematic errors from lattice spacing and the volume are negligible also for $\alpha - \beta$. From this, we can expect that those errors on individual α, β and, further, the relevant form factor W_0 are negligible compared to the other errors.

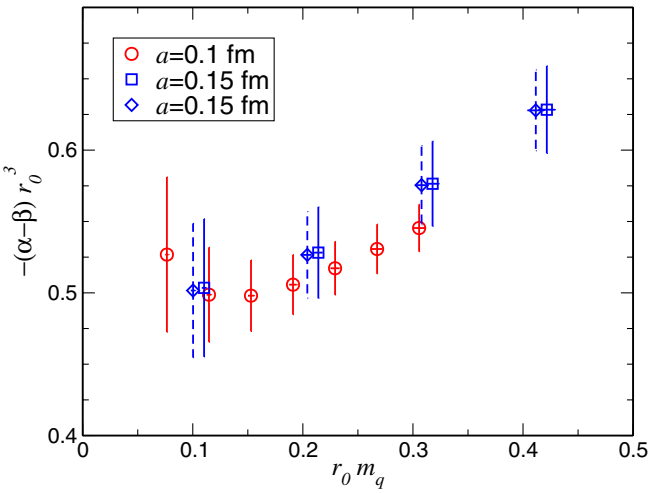

FIG. 13 (color online). The difference of the nucleon-decay low-energy parameter $-(\alpha - \beta)$ (taking the signs of α and β from the previously described extraction) as a function of quark mass. Both axes are normalized using r_0. Circles ($a = 0.1$ fm) and squares ($a = 0.15$ fm) are obtained using Eq. (64), while diamonds ($a = 0.15$ fm) are from Eq. (54) and are shifted slightly to the left for clarity. Consistent results are obtained for the different lattice spacings and different spatial volumes.

The systematic error from the chiral extrapolation may be caused by the linear extrapolation in quark mass, while, in general, contribution of higher order terms and, in the special case of quenching (by QχPT), lower order terms may not be negligible. Our linear extrapolations for matrix elements and hadron masses (for extracting the lattice scale) have been performed for the mass region where the resulting χ^2 is small. This does not necessarily mean the leading linear dependence is sufficient. This can be the case when a term with lower power occurs at higher loops in the chiral expansion. An example of this is the ρ [67] and nucleon [68] masses, for which $m_q^{1/2}$ terms appear at one loop. The correct quenched results may only be found when using a proper QχPT formula with data sufficiently good in quality and in quantity to determine the fitting parameters. Only after that can we deal with the quench error by examining the difference to the experiment or by comparing to the unquenched results. Lack of the QχPT knowledge of the matrix elements as well as the limited quality and quantity for our data make it difficult to follow this scheme.

We observed a scale inconsistency between the ρ and nucleon mass inputs when using the linear chiral extrapolation. This difference has been taken as the systematic error to the matrix elements due to the scale ambiguity. Since the finite volume and finite lattice spacing errors are negligible, we expect that this scale error is dominated by the chiral extrapolation and quenching error. Whether this estimate is plausible or not will be examined by comparing with the results with dynamical fermion simulation, which will be discussed in the next section. Note, however, the comparison is done only at a finite lattice spacing for the unquenched calculation. While we would also expect the discretization error to be small for the unquenched calculation, this should be checked in future studies.

V. DYNAMICAL-QUARK EFFECTS

Quenched calculations have, in general, an uncontrolled systematic uncertainty. In the previous section, we estimated the systematic error due to quenching as approximately the size of scale ambiguity. This is clearly an unsatisfactory technique, and full QCD calculations are necessary. Ultimately, this can be completed by unquenching the u, d, and s quarks in the direct calculation of the form factors. As a first step toward this direction, we shall examine the low-energy parameters α and β with dynamical u and d quarks, while still treating the s quark in the quenched approximation.

A. Description of the simulation

We use the two-flavor dynamical DWF configurations described in [69]. These lattices were generated using the DBW2 gauge action with $6/g^2 = 0.8$, on lattices of size $16^3 \times 32$, a fifth dimension of $L_s = 12$, and a domain-wall height of $M_5 = 1.8$ (see Table I). A periodic boundary condition was imposed for all except the temporal direction of dynamical fermions and valence fermions for the spectrum and matrix elements, where antiperiodic boundary conditions were used. The dynamical-quark masses are $m_f^{\mathrm{dyn}} = 0.02, 0.03, 0.04$, which approximately covers the range from the half strange to strange quark mass. All the analysis was carried out for the valence masses equal to the dynamical masses, $m_f^{\mathrm{val}} = m_f^{\mathrm{dyn}}$.

For the mass and matrix element calculation, Coulomb gauge fixed wall sources were used. Measurements were performed twice per lattice: with the two source time slices separated by the half size of the temporal direction $L_\tau/2$, which effectively doubled the statistics in comparison to the analysis done in Ref. [69].

The results of the mass measurements are summarized in Table V. A linear chiral extrapolation was performed for all the quantities in the table using all three quark masses. Figure 14 shows ρ and nucleon masses and their chiral extrapolations.

The lattice spacing determined in the chiral limit by inputting $m_\rho = 0.77$ GeV is

$$a_\rho^{-1} = 1.678(40)\ \mathrm{GeV}. \tag{65}$$

This is consistent with the previous estimate, $a_\rho^{-1} = 1.691(53)$ GeV [69], obtained with a single quark propagator on each lattice. The error has been reduced as ex-

TABLE V. m_{res}, Z_A, and hadron masses from the wall source propagator for two-flavor dynamical domain-wall fermions with $6/g^2 = 0.8$ DBW2 gauge action. Two quark propagators with different source positions are analyzed for each configuration. The nucleon-decay low-energy parameters α and β for the bare operator in lattice units are also shown. We have performed a linear chiral extrapolation for all quantities using all dynamical masses, $m_f = 0.02, 0.03, 0.04$. The chiral limit is defined as $m_f \to -m_{\mathrm{res}}$, except $m_f \to 0$ for m_{res}. For m_π, squared values are fit and the chiral limit shows the extrapolated m_π^2.

m_f	$m_{\mathrm{res}}(\times 10^{-3})$	Z_A	m_π	m_ρ	m_N	$\alpha(\times 10^{-3})$	$\beta(\times 10^{-3})$
0.02	1.360(26)	0.76035(27)	0.2916(15)	0.5474(50)	0.7631(88)	−4.77(25)	4.74(25)
0.03	1.357(21)	0.76187(23)	0.3563(13)	0.5991(51)	0.8383(87)	−5.27(25)	5.13(25)
0.04	1.336(24)	0.76323(21)	0.4084(22)	0.6325(52)	0.8980(92)	−5.97(31)	5.95(32)
chiral limit	1.388(55)	0.7573(6)	−0.0029(25)	0.459(11)	0.621(20)	−3.47(62)	3.43(61)
χ^2/dof	0.10/1	0.08/1	0.55/1	2.11/1	0.51/1	0.11/1	0.42/1

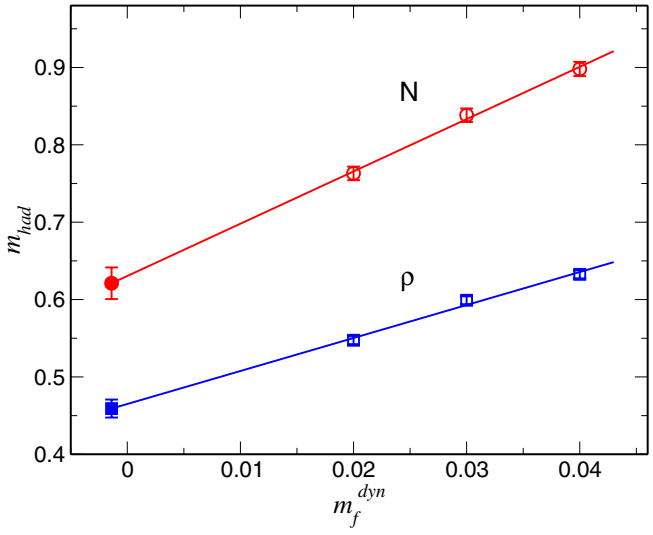

FIG. 14 (color online). ρ and nucleon masses as functions of $m_f^{\rm dyn} = m_f^{\rm val}$.

pected. For comparison, $a_{r_0}^{-1} = 1.688(21)(^{+64}_{-04})$ is obtained [69] with $r_0 = 0.5$ fm input, which is consistent with ρ input. The lattice spacing from the ρ input is $a_\rho = 0.1176(28)$ fm. Thus, the spatial size of these lattices is 1.88 fm. The spatial size divided by the pion Compton wavelength at our lightest mass is $LM_\pi \simeq 4.7$. Systematic numerical studies [70,71], as well as theoretical calculations [72], on the finite volume effects in the nucleon mass with two-flavor Wilson fermions indicate just a few percent finite volume mass shift with parameters similar to our lightest point. From this, we expect that the volume effect on the low-energy parameters is also small and negligible compared with the statistical error.

The ratio $m_N/m_\rho = 1.353(47)$ at the chiral limit is larger by 3σ from physical value 1.218. While this discrepancy is of a size that could be easily ascribed to scaling violations, it should be noted that a similar size of discrepancy for the ratio has been observed in the continuum limit of the two-flavor Wilson fermion [73] using the polynomial chiral extrapolation for the masses. This suggests that our discrepancy might persist towards the continuum limit. There is a way to cure this problem by employing the higher order chiral expansion for the nucleon mass with terms nonanalytic in the quark mass [71,74].

B. Matrix elements

For the nonperturbative renormalization of the operators, we follow the same procedure as for the quenched calculation. The dynamical mass points $m_f = 0.02$, 0.03, 0.04 are used to analyze the MOM-scheme renormalization. Linear chiral extrapolation in dynamical mass m_f is carried out. The resulting renormalization factors [Eq. (43)] which renormalize the lattice operator to give those in the $\overline{\rm MS}$, NDR scheme at $\mu = 2$ GeV are

$$U^{\overline{\rm MS}\leftarrow{\rm latt}}(2\ {\rm GeV}) = \begin{cases} 0.731(28)(39) & \text{for } \mathcal{O}^{L;L}, \\ 0.722(28)(39) & \text{for } \mathcal{O}^{R;L}, \end{cases} \quad (66)$$

where the $\Lambda_{\overline{\rm MS}}$ calculated by Alpha Collaboration for the two-flavor QCD [75], $\Lambda^{(2)}_{\overline{\rm MS}} r_0 = 0.62(4)(4)$, has been used.

The low-energy parameters are also obtained in the same way as in the quenched case, and are shown in Table V. Figure 15 shows α at the renormalization scale $\mu = 2$ GeV obtained on the dynamical configurations as a function of the pion mass squared with the scale set by ρ in the chiral limit. The quenched results are shown for comparison. The dynamical result has a stronger m_π dependence than the quenched results. After a rather long extrapolation to the chiral limit with a linear function of quark mass, we obtain the α and β parameters as

$$-\alpha = 0.0118(21)\ {\rm GeV}^3, \quad (67)$$

$$\beta = 0.0118(21)\ {\rm GeV}^3, \quad (68)$$

where errors are only statistical. Compared to these large errors, the errors of the renormalization constants are negligible. These values are consistent with those obtained in quenched approximation, Eqs. (56) and (57).

In Table VI our results on the low-energy parameters both for quenched and dynamical simulations are compared with those obtained in the literature, which include various QCD model calculations and the lattice QCD efforts by several groups. It should be remarked that the efforts of recent calculations, including this work, have substantially decreased the ambiguity of the low-energy parameters α and β. Their absolute values fall in the range of the approximate value 0.01 GeV^3, which lies in the

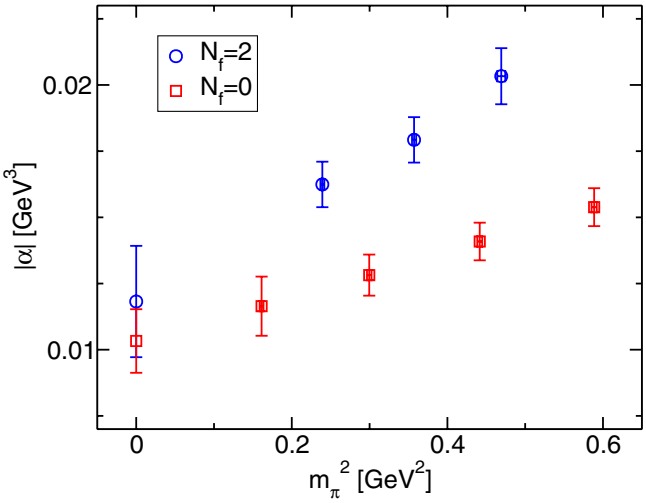

FIG. 15 (color online). Comparison of the quenched and dynamical α as a function of pion mass squared. The scale is set by the ρ input at the chiral limit. Operators are renormalized by the $\overline{\rm MS}$, NDR scheme at $\mu = 2$ GeV.

TABLE VI. Comparison of the low-energy parameter of the nucleon-decay chiral Lagrangians α and β among various QCD model calculation, lattice results in the literature and the results from this work. In lattice QCD calculations, WF and DWF mean Wilson and domain-wall fermions. Our quenched results are shown with the total error consisting of statistical and systematic errors on the bare matrix element, renormalization constant, and scale. The unquenched errors are only statistical.

		$\lvert\alpha\rvert$ (GeV^3)	$\lvert\beta\rvert$ (GeV^3)	
QCD model calculation	Donoghue and Goldwich [13]	0.003		Bag model
	Thomas and McKellar [16]	0.02		Bag model
	Meljanac *et al.* [14]	0.004		Bag model
	Ioffe [11]	0.009		Sum rule
	Krasnikov *et al.* [15]	0.003		Sum rule
	Ioffe and Smilga [17]	0.006		Sum rule
	Tomozawa [12]	0.006		Quark model
	Brodsky *et al.* [18]	0.03		
Lattice QCD $N_f = 0$	Hara *et al.* [19]	0.03		WF, $a = 0.11$ fm
	Bowler *et al.* [20]	0.013	0.010	WF, $a = 0.22$ fm
	Gavela *et al.* [21]	0.0056(8)	$\simeq \lvert\alpha\rvert$	WF, $a = 0.09$ fm
	JLQCD [22]	0.015(1)	0.014(1)	WF, $a = 0.09$ fm
	CP-PACS & JLQCD [23]	$0.0090(09)(^{+5}_{-19})$	$0.0096(09)(^{+6}_{-20})$	WF, continuum limit
	This work	0.0100(19)	0.0108(21)	DWF, $a = 0.15$ fm
Lattice QCD $N_f = 2$	This work	0.0118(21)	0.0118(21)	DWF, $a = 0.12$ fm

middle of the wide range of the various QCD model calculation results, 0.003–0.03 GeV^3.

VI. CONCLUSIONS

Using domain-wall fermions and a nonperturbative renormalization, we have calculated the low-energy matrix elements of the nucleon decay whose operator would appear in the lowest order, low-energy effective Hamiltonian of any fundamental high-energy theory that breaks baryon number and respects the symmetries of the standard model at low energies.

The low-energy parameters α and β are important fundamental quantities of the $SU(3)_f$ baryon chiral Lagrangian with the baryon number violating interaction. In the quenched approximation they were estimated at our lattice spacing ($a \simeq 1.5$ fm) as $\alpha = -0.0100(19)$, $\beta = 0.0108(21)$ GeV^3 for the operator renormalized at $\mu = 2$ GeV. We have examined the finite volume and finite lattice spacing effects on $\alpha - \beta$, which appeared to be negligible. These results are consistent with those using Wilson fermions in the continuum limit [23]. The dynamical-quark effects on α and β were examined by unquenching u and d quarks. Their values at the chiral limit are consistent with those in the quenched approximation. All the results so far indicate $|\alpha| \simeq |\beta| \simeq 0.01$ GeV^3, which lies in the middle of the various model calculations (0.003–0.03 GeV^3).

However, these parameters are not quite useful for the physical decay process. The results of the nucleon-decay form factors calculated with α and β showed clear deviation from the direct calculation for several processes. This is presumably due to the large energy of the pseudoscalar meson, and because of neglecting some leading quark mass dependent terms in the chiral Lagrangian. Instead, it is advised to use the results with the direct calculation (Table IV) for the partial width of the proton, Eq. (18). The value of the form factor with the direct method tends to be smaller compared to the indirect method; thus the direct method, which is more accurate, tends to prolong the proton lifetime. Indeed, for the case of $p \to e^+ + \pi^0$, which is important experimentally especially for a model independent analysis such as Ref. [76], the difference in our central values (with appreciable error bars) for the form factors tends to approach a factor of about 2. It is clearly important to improve the precision of the direct method in future calculations.

The dynamical-quark effects on the low-energy parameters were apparent only for their enhanced mass dependence. However, this calculation was performed at a single lattice spacing, and with only two—relatively heavy—dynamical quarks. A clear target for the future is to repeat this calculation with three flavors of dynamical quarks with masses near the physical values and multiple lattice spacings.

ACKNOWLEDGMENTS

We thank N. Christ and B. Mawhinney for the continuous support of this study. Discussions with them as well as with T. Blum, T. Izubuchi, K. Orginos, S. Ohta, and N. Yamada are gratefully acknowledged. We thank T. Izubuchi, again, for checking the calculation of the low-energy constants of proton decay for the dynamical-quark simulation. The calculations reported here were done on the 400 Gflops QCDSP computer [80] at Columbia

University and the 600 Gflops QCDSP computer [81] at the RIKEN-BNL Research Center. We thank RIKEN, Brookhaven National Laboratory and the U.S. Department of Energy for providing the facilities essential for the completion of this work. This research was supported in part by the DOE under Grant No. DE-AC02-98CH10886 (Soni).

APPENDIX A: FIELDS AND CONVENTION

In this appendix, various conventions in our calculation are summarized.

Let $\vec{p}$ and $\vec{k}$ be spatial momenta and i and j symbolically denote the other discrete quantum numbers; the state normalization is given by

$$\langle \vec{p}, i|\vec{k}, j\rangle = (2\pi)^3 2E(\vec{p}, i)\delta^3(\vec{k} - \vec{p})\delta_{i,j}, \tag{A1}$$

where $E(\vec{p}, i)$ is the energy of the $(\vec{p}, i)$ state.

The spin $1/2$ wave function $u_N(k, s)$ with momentum k, spin s, and mass m, which obeys the Dirac equation $(-i\not{k}u_N = mu_N)$, has a relativistic normalization,

$$\bar{u}_N(k, s)u_N(k, s') = 2m\delta_{s,s'}. \tag{A2}$$

Hadron interpolation fields, J_{Had}, are given as

$$J_{\pi^0} = \frac{1}{\sqrt{2}}(\bar{u}\gamma_5 u - \bar{d}\gamma_5 d), \tag{A3}$$

$$J_{\pi^+} = \bar{d}\gamma_5 u, \tag{A4}$$

$$J_{\pi^-} = \bar{u}\gamma_5 d, \tag{A5}$$

$$J_{K^0} = \bar{s}\gamma_5 d, \tag{A6}$$

$$J_{K^+} = \bar{s}\gamma_5 u, \tag{A7}$$

$$J_{\eta} = \frac{1}{\sqrt{6}}(\bar{u}\gamma_5 u + \bar{d}\gamma_5 d - 2\bar{s}\gamma_5 s), \tag{A8}$$

$$J_p = \epsilon_{ijk}(u^{iT}C\gamma_5 d^j)u^k, \tag{A9}$$

$$J_n = \epsilon_{ijk}(u^{iT}C\gamma_5 d^j)d^k. \tag{A10}$$

APPENDIX B: CHIRAL PERTURBATION

We use the tree-level chiral perturbation theory for the nucleon-decay matrix elements [22,32]. The strong interaction chiral Lagrangian of $SU(3)_f$ octet baryons has coupling constants D and F describing the coupling of the nucleon to the axial current, and a_i, b_i $(i = 1, 2)$ governing the leading linear quark mass dependence. The nucleon-decay specific term is proportional to α or β that we are calculating on the lattice.

The low-energy parameters D and F can be related to the axial charge associated with the baryon semileptonic beta decay. $D + F = g_A^{(np)} = 1.27$ is the nucleon axial charge, while $D - F = g_A^{(\Sigma^- n)} = 0.33$–$0.34$ can be measured by $\Sigma^- \to n + e^- + \bar{\nu}_e$ [77,78]. a_i are determined by the mass difference of the baryons, and the size is $O(1)$. For the nucleon-decay matrix element, a_i enter through the baryon masses. While b_i have direct influence on the nucleon-decay amplitude, their values are not well known. Although they can naturally be $O(1)$, we set them to zero in the following.

Here is the summary of the value of parameters we employed,

$$D = 0.8, \tag{B1}$$

$$F = 0.47, \tag{B2}$$

$$f = 0.131 \text{ GeV}, \tag{B3}$$

$$m_N = 0.94 \text{ GeV}, \tag{B4}$$

$$m_B = 1.15 \text{ GeV}, \tag{B5}$$

where m_B is the average baryon mass $m_B \simeq M_\Sigma \simeq M_\Lambda$.

Using these constants and the approximations $m_{u,d} \ll m_s \ll m_{N,B}$, $-q^2 \ll m_{N,B}^2$, the relevant form factors $\langle PS|\mathcal{O}|N\rangle_0 \equiv W_0$ of all the principal matrix elements are obtained as

$$\langle \pi^0|(u, d)_R u_L|p\rangle_0 = \frac{\alpha}{\sqrt{2}f}(1 + D + F), \tag{B6}$$

$$\langle \pi^0|(u, d)_L u_L|p\rangle_0 = \frac{\beta}{\sqrt{2}f}(1 + D + F), \tag{B7}$$

$$\langle K^0|(u, s)_R u_L|p\rangle_0 = -\frac{\alpha}{f}\left(1 + (D - F)\frac{m_N}{m_B}\right), \tag{B8}$$

$$\langle K^0|(u, s)_L u_L|p\rangle_0 = \frac{\beta}{f}\left(1 - (D - F)\frac{m_N}{m_B}\right), \tag{B9}$$

$$\langle K^+|(u, s)_R d_L|p\rangle_0 = \frac{\alpha}{f}\frac{2D}{3}\frac{m_N}{m_B}, \tag{B10}$$

$$\langle K^+|(u, s)_L d_L|p\rangle_0 = \frac{\beta}{f}\frac{2D}{3}\frac{m_N}{m_B}, \tag{B11}$$

$$\langle K^+|(u, d)_R s_L|p\rangle_0 = \frac{\alpha}{f}\left(1 + \left(\frac{D}{3} + F\right)\frac{m_N}{m_B}\right), \tag{B12}$$

$$\langle K^+|(u, d)_L s_L|p\rangle_0 = \frac{\beta}{f}\left(1 + \left(\frac{D}{3} + F\right)\frac{m_N}{m_B}\right), \tag{B13}$$

$$\langle K^+|(d, s)_R u_L|p\rangle_0 = \frac{\alpha}{f}\left(1 + \left(\frac{D}{3} - F\right)\frac{m_N}{m_B}\right), \tag{B14}$$

$$\langle K^+|(d,s)_L u_L|p\rangle_0 = -\frac{\beta}{f}\left(1-\left(\frac{D}{3}-F\right)\frac{m_N}{m_B}\right), \quad \text{(B15)}$$

$$\langle \eta|(u,d)_R u_L|p\rangle_0 = -\frac{\alpha}{\sqrt{6}f}(1+D-3F), \quad \text{(B16)}$$

$$\langle \eta|(u,d)_L u_L|p\rangle_0 = \frac{\beta}{\sqrt{6}f}(3-D+3F). \quad \text{(B17)}$$

Nucleon to pseudoscalar and nucleon to vacuum matrix elements are related in the zero momentum limit of the pseudoscalar by the soft pion theorem,

$$\lim_{p_\mu\to 0}\langle \pi^k; p_\mu|\mathcal{O}|N\rangle = -\frac{i}{f}\langle 0|[Q_5^k, \mathcal{O}]|N\rangle. \quad \text{(B18)}$$

Q_5^k is the axial charge having the same $SU(3)$ flavor content as the π^k pion. It is one of the pseudoscalar states: $\pi^{0,+,-}$, $K^{0,+}$, η, as we can consider an ideal situation, massless limit of all of them.

From Eq. (16), the matrix element in the soft pion limit is written in terms of the form factors as

$$\lim_{p_\mu\to 0}\langle PS; p_\mu|\mathcal{O}^L|N\rangle = P_L[W_0 + m_N W_q]u_N. \quad \text{(B19)}$$

In the following, relations for $\langle PS|\mathcal{O}|N\rangle_{sp} \equiv W_0 + m_N W_q$ are obtained by the soft pion theorem, Eq. (B18), or by the $p_\mu \to 0$ limit of the tree-level results of the chiral perturbation theory.

$$\langle \pi^0|(u,d)_R u_L|p\rangle_{sp} = \frac{\alpha}{\sqrt{2}f}, \quad \text{(B20)}$$

$$\langle \pi^0|(u,d)_L u_L|p\rangle_{sp} = \frac{\beta}{\sqrt{2}f}, \quad \text{(B21)}$$

$$\langle K^0|(u,s)_R u_L|p\rangle_{sp} = -\frac{\alpha}{f}, \quad \text{(B22)}$$

$$\langle K^0|(u,s)_L u_L|p\rangle_{sp} = \frac{\beta}{f}, \quad \text{(B23)}$$

$$\langle K^+|(u,s)_R d_L|p\rangle_{sp} = 0, \quad \text{(B24)}$$

$$\langle K^+|(u,s)_L d_L|p\rangle_{sp} = 0, \quad \text{(B25)}$$

$$\langle K^+|(u,d)_R s_L|p\rangle_{sp} = \frac{\alpha}{f}, \quad \text{(B26)}$$

$$\langle K^+|(u,d)_L s_L|p\rangle_{sp} = \frac{\beta}{f}, \quad \text{(B27)}$$

$$\langle K^+|(d,s)_R u_L|p\rangle_{sp} = \frac{\alpha}{f}, \quad \text{(B28)}$$

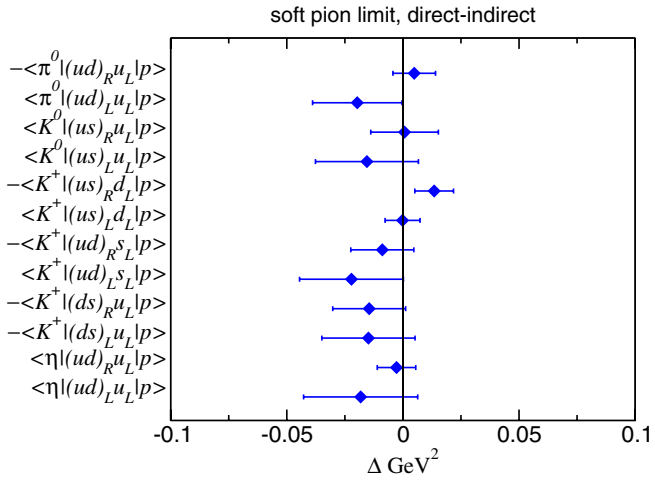

FIG. 16 (color online). The difference Δ of the form factors for direct and indirect methods in the soft pion limit. It shows the consistency with the soft pion theorem.

$$\langle K^+|(d,s)_L u_L|p\rangle_{sp} = -\frac{\beta}{f}, \quad \text{(B29)}$$

$$\langle \eta|(u,d)_R u_L|p\rangle_{sp} = -\frac{\alpha}{\sqrt{6}f}, \quad \text{(B30)}$$

$$\langle \eta|(u,d)_L u_L|p\rangle_{sp} = \frac{3\beta}{\sqrt{6}f}. \quad \text{(B31)}$$

These exact relations no longer involve any ordinary low-energy baryonic constants. Checking these relations with the lattice simulation provides a consistency test of the whole procedure. We have measured $W_0 - iq_4 W_q$ with zero pseudoscalar momentum and degenerate masses for the lhs. The chiral limit should be taken with

$$W_0 - iq_4 W_q = c_0 + c_1 m_q + c_h\sqrt{m_q}. \quad \text{(B32)}$$

The square root of the quark mass ($\propto m_\pi$) has entered from q^2 dependence. Together with α and β [Eqs. (56) and (57)], the difference Δ = lhs − rhs is calculated and shown in Fig. 16. Most of the processes are consistent with $\Delta = 0$ (note that these are highly correlated values). Even in the worst case, the deviation is less than 2σ.

APPENDIX C: PERTURBATIVE MATCHING FACTOR

Here we give a summary of the nucleon-decay operator matching calculation. Throughout, we make use of the Minkowski space path integral. We need to match to the lattice MOM scheme with the continuum $\overline{\text{MS}}$ scheme. Since the MOM scheme is regularization independent, we can use perturbation theory in both schemes. In the lattice MOM scheme, the same momentum p_μ^E is injected into all the three quark external lines, where $(p^E)^2 > 0$. The corresponding Minkowski momentum is $(p^M)^2 = -(p^E)^2 < 0$. Both the $\overline{\text{MS}}$ and MOM schemes are defined

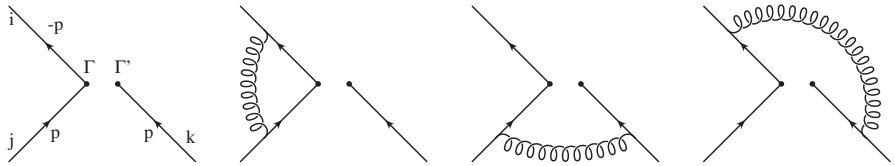

FIG. 17. The tree and one-loop diagrams of the vertex function for $\epsilon^{ijk}(\bar{u}^{ci}\Gamma d^j)\Gamma' s^k$.

in the massless limit. We set all masses to zero for the MOM scheme in perturbation theory.

The tree-level vertex function is

$$\Lambda_{\rm ND}^{(0)} = \epsilon^{ijk}\Gamma \otimes \Gamma', \tag{C1}$$

where Γ and Γ' can be either 1 or γ_5 or their linear combinations. The corresponding Feynman diagram is shown in Fig. 17 (leftmost). The upper left fermion line is for the charge conjugated field, whose vertex for one gluon emission is $-ig(t^a)^T$, whereas the normal vertex is igt^a.

The sum of the three one-loop diagrams in Fig. 17 with the NDR scheme reads

$$\Lambda_{\rm ND}^{(1)} = \int \frac{d^4k}{(2\pi)^4} i\frac{2}{3} g^2 \mu^{2\varepsilon} \epsilon^{ijk}[\lambda^F + (1-\xi)\lambda^{L-F}], \tag{C2}$$

where μ is the arbitrary mass scale introduced by the dimensional regularization, $\varepsilon = (4-D)/2$, D is the regularized dimension, and ξ is the gauge parameter ($\xi = 0$ is the Landau gauge). λ^F and λ^{L-F} read

$$\lambda^F = \frac{(D+2)(p^2-k^2)\Gamma\otimes\Gamma'}{[(p-k)^2+i\epsilon][(p+k)^2+i\epsilon][k^2+i\epsilon]}, \tag{C3}$$

$$\begin{aligned}\lambda^{L-F} = {} & \frac{3\Gamma\otimes\Gamma'}{[(p-k)^2+i\epsilon][(p+k)^2+i\epsilon]} \\ & - \frac{p^2\Gamma\otimes\Gamma'}{[(p-k)^2+i\epsilon][(p+k)^2+i\epsilon][k^2+i\epsilon]} \\ & - \frac{2(p\cdot k)\Gamma\otimes\Gamma' \not{p}\not{k}}{[(p-k)^2+i\epsilon][(p+k)^2+i\epsilon][k^2+i\epsilon]^2}.\end{aligned} \tag{C4}$$

Carrying out the momentum integral and identifying μ^2 with $-p^2$, one finally finds

$$\begin{aligned}\Lambda_{\rm ND}^{(1)} = \frac{\alpha_s}{4\pi}\Bigg\{ & [4-2(1-\xi)]\bar{\varepsilon}^{-1} + \left(\frac{20}{3} - 16\ln 2\right) \\ & - (1-\xi)\left(\frac{767}{180} - \frac{317}{90}\ln 2\right)\Bigg\}\Lambda_{\rm ND}^{(0)},\end{aligned} \tag{C5}$$

where $\bar{\varepsilon}^{-1} = 2/(4-D) - \gamma_E + \ln 4\pi$. The renormalization condition of the MOM scheme up to one loop reads

$$\Lambda_{\rm ND}^{(0)} = (Z_q^{\rm MOM})^{-3/2} Z_{\rm ND}^{\rm MOM}(\Lambda_{\rm ND}^{(0)} + \Lambda_{\rm ND}^{(1)}). \tag{C6}$$

The MOM-scheme quark wave function renormalization is given as (see, for example, [79])

$$Z_q^{\rm MOM} = 1 + \frac{\alpha_s}{4\pi}\left[\frac{4}{3}(-\xi)\bar{\varepsilon}^{-1} + \frac{2}{3}(-\xi)\right]. \tag{C7}$$

Then the nucleon-decay operator renormalization factor is calculated as

$$\begin{aligned}Z_{\rm ND}^{\rm MOM} = 1 + \frac{\alpha_s}{4\pi}\Bigg[& 2\bar{\varepsilon}^{-1} + \frac{433}{180} - \frac{1123}{90}\ln 2 \\ & + \xi\left(\frac{587}{180} - \frac{317}{90}\ln 2\right)\Bigg].\end{aligned} \tag{C8}$$

The $\overline{\rm MS}$ renormalization factor is given by taking only the term proportional to $\bar{\varepsilon}^{-1}$ in the square brackets. The matching renormalization factor $Z^{\overline{\rm MS}}/Z^{\rm MOM}$ has been shown in Eq. (49).

TABLE VII. Relevant form factor W_0 of the principal matrix elements with the unrenormalized operator for each mass and momentum calculated on the quenched $a = 0.15$ fm configurations. $\vec{p}_1 = (1,0,0)\cdot 2\pi/L_\sigma$ is for the smallest and $\vec{p}_2 = (1,1,0)\cdot 2\pi/L_\sigma$ is for the second smallest momentum.

		RL operator		*LL* operator	
m_1	m_2	$\vec{p}=\vec{p}_1$	$\vec{p}=\vec{p}_2$	$\vec{p}=\vec{p}_1$	$\vec{p}=\vec{p}_2$
		$\langle\pi^0\vert(ud)u\vert p\rangle$			
0.02	0.02	−0.053(15)	0.051 (44)	0.061 (19)	0.057 (72)
0.02	0.04	−0.060(12)	0.009 (21)	0.065 (14)	0.055 (35)
0.02	0.06	−0.064(11)	−0.011(15)	0.067 (13)	0.059 (24)
0.02	0.08	−0.066(11)	−0.023(13)	0.069 (12)	0.060 (18)
0.04	0.04	−0.071(8)	−0.036(10)	0.075 (8)	0.061 (14)
0.04	0.06	−0.073(7)	−0.042(8)	0.075 (7)	0.060 (10)
0.04	0.08	−0.073(6)	−0.047(7)	0.074 (7)	0.061 (8)
0.06	0.06	−0.082(6)	−0.056(7)	0.082 (6)	0.064 (7)
0.06	0.08	−0.081(5)	−0.058(6)	0.080 (5)	0.064 (6)
0.08	0.08	−0.088(5)	−0.065(5)	0.086 (5)	0.068 (5)
		$\langle K^0\vert(us)u\vert p\rangle$			
0.02	0.02	0.054 (13)	0.050 (43)	0.035 (14)	0.019 (49)
0.02	0.04	0.056 (11)	0.035 (22)	0.036 (10)	0.016 (24)
0.02	0.06	0.057 (11)	0.035 (17)	0.039 (9)	0.019 (17)
0.02	0.08	0.059 (10)	0.038 (14)	0.042 (8)	0.023 (14)
0.04	0.04	0.065 (7)	0.045 (11)	0.031 (5)	0.017 (10)
0.04	0.06	0.066 (7)	0.047 (9)	0.034 (4)	0.024 (8)
0.04	0.08	0.066 (6)	0.050 (8)	0.037 (4)	0.029 (6)
0.06	0.06	0.069 (5)	0.053 (7)	0.033 (3)	0.029 (5)
0.06	0.08	0.069 (5)	0.055 (6)	0.036 (3)	0.033 (4)
0.08	0.08	0.072 (4)	0.058 (5)	0.036 (2)	0.034 (4)

TABLE VIII. Continued from Table VII.

m_1	m_2	*RL* operator $\vec{p}=\vec{p}_1$	*RL* operator $\vec{p}=\vec{p}_2$	*LL* operator $\vec{p}=\vec{p}_1$	*LL* operator $\vec{p}=\vec{p}_2$
		$\langle K^+\|(us)d\|p\rangle$			
0.02	0.02	−0.020(9)	0.013 (29)	0.017 (10)	0.017 (35)
0.02	0.04	−0.020(7)	0.002 (13)	0.018 (7)	0.015 (16)
0.02	0.06	−0.020(6)	−0.001(9)	0.019 (6)	0.016 (11)
0.02	0.08	−0.019(5)	−0.003(8)	0.018 (5)	0.017 (8)
0.04	0.04	−0.029(4)	−0.013(6)	0.025 (3)	0.021 (6)
0.04	0.06	−0.028(4)	−0.014(4)	0.024 (3)	0.018 (4)
0.04	0.08	−0.027(3)	−0.014(4)	0.023 (3)	0.017 (3)
0.06	0.06	−0.033(3)	−0.019(3)	0.027 (2)	0.019 (3)
0.06	0.08	−0.031(3)	−0.019(3)	0.026 (2)	0.018 (3)
0.08	0.08	−0.035(2)	−0.023(2)	0.029 (2)	0.020 (2)
		$\langle K^+\|(ud)s\|p\rangle$			
0.02	0.02	−0.056(17)	0.067 (48)	0.068 (19)	0.073 (74)
0.02	0.04	−0.065(14)	0.011 (22)	0.073 (15)	0.067 (37)
0.02	0.06	−0.070(13)	−0.014(16)	0.076 (13)	0.069 (25)
0.02	0.08	−0.074(12)	−0.031(14)	0.079 (12)	0.070 (20)
0.04	0.04	−0.072(8)	−0.038(11)	0.081 (8)	0.066 (15)
0.04	0.06	−0.075(7)	−0.047(9)	0.082 (7)	0.067 (11)
0.04	0.08	−0.077(7)	−0.053(8)	0.083 (7)	0.069 (9)
0.06	0.06	−0.082(6)	−0.060(7)	0.088 (6)	0.071 (7)
0.06	0.08	−0.083(6)	−0.063(7)	0.088 (6)	0.072 (7)
0.08	0.08	−0.090(5)	−0.069(6)	0.093 (5)	0.076 (6)

TABLE IX. Continued from Table VIII.

m_1	m_2	*RL* operator $\vec{p}=\vec{p}_1$	*RL* operator $\vec{p}=\vec{p}_2$	*LL* operator $\vec{p}=\vec{p}_1$	*LL* operator $\vec{p}=\vec{p}_2$
		$\langle K^+\|(ds)u\|p\rangle$			
0.02	0.02	−0.034(9)	−0.058(43)	−0.051(14)	−0.065(54)
0.02	0.04	−0.035(7)	−0.038(22)	−0.054(11)	−0.050(27)
0.02	0.06	−0.037(7)	−0.035(16)	−0.057(9)	−0.050(19)
0.02	0.08	−0.039(6)	−0.037(13)	−0.060(9)	−0.051(15)
0.04	0.04	−0.035(5)	−0.033(10)	−0.056(6)	−0.043(11)
0.04	0.06	−0.037(4)	−0.034(8)	−0.058(5)	−0.047(8)
0.04	0.08	−0.039(4)	−0.036(7)	−0.060(5)	−0.050(7)
0.06	0.06	−0.036(3)	−0.033(5)	−0.061(4)	−0.050(6)
0.06	0.08	−0.038(3)	−0.036(5)	−0.062(4)	−0.053(5)
0.08	0.08	−0.037(2)	−0.035(4)	−0.065(4)	−0.055(4)
		$\langle \eta\|(ud)u\|p\rangle$			
0.02	0.02	0.013 (7)	0.072 (42)	0.062 (17)	0.079 (66)
0.02	0.04	0.011 (5)	0.035 (19)	0.066 (13)	0.061 (32)
0.02	0.06	0.010 (5)	0.023 (13)	0.070 (11)	0.061 (23)
0.02	0.08	0.009 (5)	0.018 (11)	0.073 (11)	0.063 (18)
0.04	0.04	0.010 (3)	0.016 (8)	0.068 (7)	0.053 (13)
0.04	0.06	0.010 (3)	0.014 (6)	0.071 (6)	0.057 (10)
0.04	0.08	0.011 (2)	0.013 (5)	0.074 (6)	0.061 (8)
0.06	0.06	0.009 (2)	0.010 (4)	0.075 (5)	0.061 (7)
0.06	0.08	0.009 (2)	0.011 (3)	0.076 (5)	0.065 (6)
0.08	0.08	0.008 (1)	0.009 (2)	0.079 (4)	0.067 (5)

TABLE X. Fit results of the relevant form factor W_0 with Eq. (62) for the principal matrix elements. Values shown are in lattice units and by unrenormalized operators. dof = 16 for all.

	c_0	c_1	c_2	c_3	χ^2
$\langle \pi^0\|(ud)_R u_L\|p\rangle$	−0.047(13)	−0.125(31)	−0.24(13)	−0.27(8)	14 (11)
$\langle \pi^0\|(ud)_L u_L\|p\rangle$	0.067 (15)	0.070 (33)	0.09 (16)	0.09 (10)	0.6 (22)
$\langle K^0\|(us)_R u_L\|p\rangle$	0.055 (12)	0.071 (32)	0.07 (14)	0.12 (7)	1.6 (24)
$\langle K^0\|(us)_L u_L\|p\rangle$	0.026 (9)	0.023 (23)	−0.07(10)	0.19 (6)	4.5 (61)
$\langle K^+\|(us)_R d_L\|p\rangle$	−0.021(7)	−0.057(16)	−0.13(7)	−0.02(5)	4.7 (55)
$\langle K^+\|(us)_L d_L\|p\rangle$	0.023 (6)	0.030 (14)	0.07 (7)	−0.02(4)	1.9 (39)
$\langle K^+\|(ud)_R s_L\|p\rangle$	−0.046(14)	−0.116(34)	−0.18(15)	−0.35(9)	15 (12)
$\langle K^+\|(ud)_L s_L\|p\rangle$	0.072 (15)	0.069 (35)	0.06 (16)	0.15 (11)	0.4 (19)
$\langle K^+\|(ds)_R u_L\|p\rangle$	−0.033(8)	−0.010(22)	0.06 (9)	−0.10(5)	0.5 (16)
$\langle K^+\|(ds)_L u_L\|p\rangle$	−0.049(11)	−0.043(26)	0.01 (12)	−0.17(7)	0.5 (10)
$\langle \eta\|(ud)_R u_L\|p\rangle$	0.013 (6)	−0.012(15)	−0.04(6)	−0.02(4)	4.7 (66)
$\langle \eta\|(ud)_L u_L\|p\rangle$	0.061 (13)	0.053 (32)	−0.01(14)	0.20 (9)	0.5 (10)

APPENDIX D: NUMERICAL TABLES

All the results for the relevant form factor W_0 of the principal matrix elements are shown in Tables VII, VIII, and IX. The fit result of the relevant form factors with Eq. (62) is presented in Table X.

[1] J. C. Pati and A. Salam, Phys. Rev. D **8**, 1240 (1973).
[2] H. Georgi and S. L. Glashow, Phys. Rev. Lett. **32**, 438 (1974).
[3] K. Kobayashi *et al.* (Super-Kamiokande Collaboration), Phys. Rev. D **72**, 052007 (2005).
[4] H. Murayama and A. Pierce, Phys. Rev. D **65**, 055009 (2002).
[5] Note that one can still save the theory by appropriate changes in the flavor structure [6,7].
[6] B. Bajc, P. Fileviez Perez, and G. Senjanovic, Phys. Rev. D **66**, 075005 (2002).
[7] D. Emmanuel-Costa and S. Wiesenfeldt, Nucl. Phys. **B661**, 62 (2003).
[8] S. Weinberg, Phys. Rev. Lett. **43**, 1566 (1979).
[9] F. Wilczek and A. Zee, Phys. Rev. Lett. **43**, 1571 (1979).
[10] L. F. Abbott and M. B. Wise, Phys. Rev. D **22**, 2208 (1980).
[11] B. L. Ioffe, Nucl. Phys. **B188**, 317 (1981).
[12] Y. Tomozawa, Phys. Rev. Lett. **46**, 463 (1981).
[13] J. F. Donoghue and E. Goldwich, Phys. Rev. D **26**, 3092 (1982).
[14] S. Meljanac, D. Palle, I. Picek, and D. Tadic, Nucl. Phys. **B206**, 298 (1982).
[15] N. V. Krasnikov, A. A. Pivovarov, and N. N. Tavkhelidze, Pis'ma Zh. Eksp. Teor. Fiz. **36**, 272 (1982) [JETP Lett. **36**, 333 (1982)].
[16] A. W. Thomas and B. H. J. McKellar, Nucl. Phys. **B227**, 206 (1983).
[17] B. L. Ioffe and A. V. Smilga, Nucl. Phys. **B232**, 109 (1984).
[18] S. J. Brodsky, J. R. Ellis, J. S. Hagelin, and C. T. Sachrajda, Nucl. Phys. **B238**, 561 (1984).
[19] Y. Hara, S. Itoh, Y. Iwasaki, and T. Yoshie, Phys. Rev. D **34**, 3399 (1986).
[20] K. C. Bowler, D. Daniel, T. D. Kieu, D. G. Richards, and C. J. Scott, Nucl. Phys. **B296**, 431 (1988).
[21] M. B. Gavela *et al.*, Nucl. Phys. **B312**, 269 (1989).
[22] S. Aoki *et al.* (JLQCD Collaboration), Phys. Rev. D **62**, 014506 (2000).
[23] N. Tsutsui *et al.* (CP-PACS Collaboration), Phys. Rev. D **70**, 111501 (2004).
[24] S. Aoki *et al.* (CP-PACS Collaboration), Phys. Rev. Lett. **84**, 238 (2000).
[25] Y. Aoki (RBC Collaboration), Nucl. Phys. B, Proc. Suppl. **119**, 380 (2003).
[26] Y. Aoki (RBC Collaboration), Nucl. Phys. B, Proc. Suppl. **129**, 305 (2004).
[27] Y. Aoki (RBC Collaboration), Nucl. Phys. B, Proc. Suppl. **140**, 405 (2005).
[28] Abbott and Wise reduced Weinberg's six operators to these four, using a (anti)symmetric property under flavor exchange.
[29] We refer to all the $qqql$ operators as dimension six. The naming is just from the naive counting of the field dimension and has nothing to do with the origin of the operator.
[30] It requires calculating the disconnected diagram, which is challenging and demanding in the numerical simulation.
[31] From the numerical calculation where we set the nucleon at rest, we observe $W_0 \sim -iq_0 W_q$. Thus, applying the lepton spinor $\bar{v}^c$ at left, $\bar{v}^c(-i\not{q}W_q) = \bar{v}^c m_l W_q \sim \bar{v}^c m_l/q_0 \cdot W_0$. Since the q_0 is the order of the nucleon mass, $-i\not{q}W_q$ is smaller than W_0 by a factor $\sim m_l/m_N$.
[32] M. Claudson, M. B. Wise, and L. J. Hall, Nucl. Phys. **B195**, 297 (1982).
[33] S. Sasaki, T. Blum, and S. Ohta, Phys. Rev. D **65**, 074503 (2002).
[34] As stated, direct calculation of the form factor does not take into account the flavor $SU(3)$ breaking effect of η. Thus, this 200% correction can be regarded as an estimate of the systematic error of direct calculation of $\langle\eta|(ud)_R u_L|p\rangle$. The correction for $\langle\eta|(ud)_L u_L|p\rangle$ is 30%.
[35] D. B. Kaplan, Phys. Lett. B **288**, 342 (1992).
[36] Y. Shamir, Nucl. Phys. **B406**, 90 (1993).
[37] V. Furman and Y. Shamir, Nucl. Phys. **B439**, 54 (1995).
[38] T. Blum and A. Soni, Phys. Rev. D **56**, 174 (1997).
[39] T. Blum and A. Soni, Phys. Rev. Lett. **79**, 3595 (1997).
[40] T. Blum *et al.*, Phys. Rev. D **69**, 074502 (2004).
[41] A. Ali Khan *et al.* (CP-PACS Collaboration), Phys. Rev. D **64**, 114506 (2001).
[42] Y. Aoki *et al.*, Phys. Rev. D **69**, 074504 (2004).
[43] Y. Aoki *et al.*, Phys. Rev. D **73**, 094507 (2006).
[44] For the ratio of correlators given on the right-hand side of Eq. (26) to be represented by a single number, we are assuming that the effect of J_{5q} on the 4-dimensional physics is local, and we are neglecting effects of $O(a^2)$.
[45] A. Ali Khan *et al.* (CP-PACS Collaboration), Phys. Rev. D **63**, 114504 (2001).
[46] T. Takaishi, Phys. Rev. D **54**, 1050 (1996).
[47] P. de Forcrand *et al.* (QCD-TARO Collaboration), Nucl. Phys. **B577**, 263 (2000).
[48] As with the extraction of the residual mass, for this equation to be true we are assuming locality and neglecting $O(a^2)$ effects, and so there is some minimum value of t before which Z_A may not be extracted.
[49] G. P. Lepage and P. B. Mackenzie, Phys. Rev. D **48**, 2250 (1993).
[50] G. Martinelli, C. Pittori, C. T. Sachrajda, M. Testa, and A. Vladikas, Nucl. Phys. **B445**, 81 (1995).
[51] T. Blum *et al.*, Phys. Rev. D **66**, 014504 (2002).
[52] T. Blum *et al.* (RBC Collaboration), Phys. Rev. D **68**, 114506 (2003).
[53] T. Nihei and J. Arafune, Prog. Theor. Phys. **93**, 665 (1995).
[54] In this notation, the $P\Gamma'$ operator consists of the scalar diquark.
[55] A typo in [53] corrected by private communication with Nihei.
[56] S. Capitani, M. Luscher, R. Sommer, and H. Wittig (ALPHA Collaboration), Nucl. Phys. **B544**, 669 (1999).
[57] R. Sommer, Nucl. Phys. **B411**, 839 (1994).
[58] It should be noted that we do not ascribe the nonvanishing values to be a consequence of explicit chiral symmetry breaking due to a finite fifth dimension, but a combination of low-energy spontaneous chiral symmetry breaking effects and discretization errors.
[59] Another way to estimate the truncation error is to guess from the difference between LO and NLO. It is about 15%, which can be seen in Fig. 4. The difference between NLO and NNLO is then estimated by taking a square to be 2%. This is the same order as, but smaller than, the 5% that we have employed.
[60] Y. Kuramashi, M. Fukugita, H. Mino, M. Okawa, and A. Ukawa, Phys. Rev. Lett. **72**, 3448 (1994).

[61] S. Sasaki, K. Orginos, S. Ohta, and T. Blum (RIKEN-BNL-Columbia-KEK Collaboration), Phys. Rev. D **68**, 054509 (2003).
[62] Instead of α (β), one can use α/f_π (β/f_π) defined at finite mass for the extrapolation. This method has an advantage of making the mass dependence milder. With our measurement, however, it makes only up to a 2% difference in the extrapolated values and up to a 10% difference in the statistical error. Apart from the way it is extrapolated, this ratio in the chiral limit might be more useful than the original, since α or β enters the form factors [Eqs. (20), (21), and (B6)–(B17)] always through the ratio with f_π. Also, since the ratio has one dimension less than the original, the scaling violation is expected to be smaller. Thus, taking the continuum limit with this ratio has an advantage in the discretization where the scaling violation is larger than the present calculation.
[63] S. Elitzur, Phys. Rev. D **12**, 3978 (1975).
[64] JLQCD [22] included a q^4 term. With our data, the effect of including such a term is to shift c_0 within one-third of the statistical error. The χ^2/dof of the uncorrelated fit increases slightly by eliminating the q^4 term, while the relative error of χ^2 estimated by jackknife remains almost unchanged.
[65] K. Hashimoto and T. Izubuchi (RBC Collaboration), Nucl. Phys. B, Proc. Suppl. **140**, 341 (2005).
[66] C. Dawson (RBC Collaboration), Nucl. Phys. B, Proc. Suppl. **119**, 314 (2003).
[67] M. Booth, G. Chiladze, and A. F. Falk, Phys. Rev. D **55**, 3092 (1997).
[68] J. N. Labrenz and S. R. Sharpe, Phys. Rev. D **54**, 4595 (1996).
[69] Y. Aoki *et al.*, Phys. Rev. D **72**, 114505 (2005).
[70] B. Orth, T. Lippert, and K. Schilling, Phys. Rev. D **72**, 014503 (2005).
[71] A. Ali Khan *et al.* (QCDSF-UKQCD Collaboration), Nucl. Phys. **B689**, 175 (2004).
[72] S. R. Beane, Phys. Rev. D **70**, 034507 (2004).
[73] A. Ali Khan *et al.* (CP-PACS Collaboration), Phys. Rev. D **65**, 054505 (2002); **67**, 059901(E) (2003).
[74] M. Procura, T. R. Hemmert, and W. Weise, Phys. Rev. D **69**, 034505 (2004).
[75] M. Della Morte *et al.* (ALPHA Collaboration), Nucl. Phys. **B713**, 378 (2005).
[76] I. Dorsner and P. F. Perez, Phys. Lett. B **625**, 88 (2005).
[77] S. Y. Hsueh *et al.*, Phys. Rev. D **38**, 2056 (1988).
[78] S. Eidelman *et al.* (Particle Data Group), Phys. Lett. B **592**, 1 (2004).
[79] E. Franco and V. Lubicz, Nucl. Phys. **B531**, 641 (1998).
[80] D. Chen *et al.*, Nucl. Phys. B, Proc. Suppl. **73**, 898 (1999).
[81] R. D. Mawhinney, Parallel Computing **25**, 1281 (1999).